수의학석사학위논문

숙신산에 의한 DRP1 인산화에 의해 유도되는 미토콘드리아 분절이 인간 중간엽 줄기세포 이동에 미치는 영향

The role of succinate-induced DRP1-mediated mitochondrial fission in human mesenchymal stem cell migration

2017년 8월

서울대학교 대학원

수의학과 수의생명과학 전공

고 소 희

ABSTRACT

The role of succinate-induced DRP1-mediated mitochondrial fission in human mesenchymal stem cell migration

So Hee Ko

Major in Veterinary Biomedical science

Department of Veterinary Medicine

The Graduate School

Seoul National University

The roles of metabolites produced from stem cell metabolism alterations have been emerging as signaling molecules to regulate stem cell behaviors such as proliferation and migration. The mitochondrial morphology is closely associated with the metabolic balance and stem cell function. However, the physiological role of succinate on human mesenchymal stem cell (hMSC) migration by regulating the mitochondrial morphology remains unclear. Here, I

investigate the underlying mechanism of succinate on the regulation of mitochondrial dynamic proteins and subsequent hMSC migration. Succinate (50 μM) significantly accelerated hMSC migration, which was inhibited by *succinate receptor1* (*gpr91*) siRNA transfection. Succinate increased phosphorylation of pan-PKC, especially the atypical PKCζ level which was blocked by the knockdown of Gα_q and G$\alpha_{12.}$ Activated PKCζ subsequently phosphorylated p38 MAPK, which was inhibited by staurosporine. Cytosolic DRP1 was phosphorylated by p38 MAPK and results in DRP1 translocation to the mitochondria outer membrane, eventually inducing mitochondrial fission. After mitochondrial fission, succinate increased ATP levels, the mitochondrial membrane potential ($\Delta\psi_m$), and mitochondrial ROS (mtROS) and they were attenuated by drp1 gene silencing. Subsequently, the elevated mtROS levels activated Rho GTPases and induced F-actin formation. Furthermore, in a skin excisional wound model, I found effects of succinate-pretreated hMSC enhanced wound closure, vascularization and re-epithelialization which were attenuated by the silencing of *drp1.* In conclusion, succinates promote DRP1-mediated mitochondrial fission via GPR91-dependent PKCζ/p38 MAPK activation which stimulates

hMSC migration through mtROS/Rho GTPase-induced F-actin formation.

Keywords: Succinate, GPR91, Mitochondrial dynamics, DRP1, p38 MAPK, ROS, Human mesenchymal stem cell

Student Number: 2015-21807

CONTENTS

LIST OF FIGURES

ABBREVIATIONS

NAC	N-acetyl-L-cysteine
ATP	Adenosine triphosphate
MSC	Mesenchymal stem cell
DRP1	Dynamin-related protein
FIS1	Mitochondrial fission protein1
MFN1/2	Mmitofusin1/2
OPA1	Optic atrophy1
MEM- α	Minimum essential medium eagle alpha Modifications
PBS	Phosphate buffered solution
FBS	Fetal bovine serum
RT	Room temperature
PCR	Polymerase chain reaction
PVDF	Polyvinylidene fluoride
FACS	Fluorescence-activated cell sorting
GTP γ S	Guanosine 5' -[γ -^{35}S]-triphosphate
GDP	Guanosine diphosphate

MAPK	Mitogen-activated protein kinase
ROD	Relative optical density
DCF-DA	2',7'-dichlorodihydrofluorescein diacetate
TMRE	Tetramethylrhodamine ethyl ester
CCCP	Carbonyl cyanide 3'-chlorophenylhydrazone
HNA	Human nuclear antigen
PI	Propidium iodide

INTRODUCTION

Stem cell metabolism delicately regulates the balance of the metabolic needs associated with the cellular state through aerobic glycolysis, glutamine catabolism, and *de novo* synthesis of fatty acid and lipids(Buravkova et al., 2014; Folmes and Terzic, 2016; Lee et al., 2015). Recently, TCA cycle metabolites such as fumarate and succinate have been widely reported to play an important role in maintaining stem cell function by adjusting their cellular ratios(Carey et al., 2015; Wanet et al., 2015). In addition to the metabolites that are used for cellular energy production, they role in cell-to-cell communication and sensing microenvironmental conditions to adapt(Wanet et al., 2015). Interestingly, metabolic intermediates have recently been found to have novel signaling functions, which have the potential to adjust stem cell behavior with regard to stem cell niche(Carey et al., 2015; TeSlaa et al., 2016). Stem cell niche, as most hypoxia, is closely associated with general

metabolic stress that is considered to be a mediator of hypoxia-induced succinate accumulation(Ejtehadifar et al., 2015; Husted et al., 2017). Furthermore, succinate has been reported to regulate the stem cell functions under the cellular physiologic condition(Ariza et al., 2012; Haas et al.; He et al., 2004). Accordingly, succinate was reported not only to be central metabolites in the cellular energy metabolism but also to regulate cell functions by initiating the signaling cascade. Extracellular succinate binds to a G-protein coupled receptor that triggers signal transduction to initiate physiological response such as cell division, capillary formation, and migration(Ariza et al., 2012; Chouchani et al., 2014; Mills and O'Neill; Mu et al., 2017; Pell et al., 2016). Thus, the comprehensive roles of succinate and its specific receptor in stem cells need to be investigated as a bioactive molecule involved in the activation of stem cell functions to facilitate tissue regeneration during wound repair process. Although this area of research is burgeoning, still numerous limitations remain, including our incomplete understanding of stem cell metabolite that has functions both in vitro and in vivo. Hence, the comprehensive roles of succinate and

those mechanisms which regulates stem cell physiology need to be investigated(Ding et al., 2015; Maxson et al., 2012).

Mitochondria are well known organelles that tightly maintain cellular homeostasis by balancing energy production and in which metabolites can accumulate during this process. Mitochondria are widespread around the cytosol and regulate various physiological functions(Cherry et al., 2016). To adapt to a new metabolic milieu, mitochondria continuously change their morphology through the fusion and fission cycle, reciprocally responding to metabolic alterations (Benard et al., 2011; Nasrallah and Horvath, 2014; Schrepfer and Scorrano, 2016). Mitochondrial dynamics are involved in various cellular functions such as redox regulation and cell proliferation(Archer, 2013). Mitochondrial fission is mostly mediated by GTPase activity on dynamin-related protein 1 (DRP1), and consequently, DRP1 translocates from the cytosol to the mitochondrial outer membrane region. On the other hand, mitochondrial fusion is mediated mainly by the optic atrophy 1 (OPA1) located on the mitochondrial outer membrane and mitofusion 1/2 (MFN1/2) located on the inner membrane(Cho et al., 2013). Although the importance of balancing the mitochondrial

morphology through mitochondrial dynamics is now understood, there is any little knowledge about the mitochondrial dynamics involved in stem cell migration. Many studies have shown that mitochondrial fission is observed in regions with high levels of energy demand, such as the axon growth axis and during oocyte maturation and cell migration(Kim et al., 2014; Yu et al., 2010). The shape and activities of proteins related to mitochondrial dynamics are mediated by post-translational modifications such as phosphorylation. Thus, efforts have been made to discover the upstream regulator of mitochondrial dynamics proteins, highlighting the emerging significance of mitochondria in stem cells(Prieto et al., 2016).

Human mesenchymal stem cells (hMSCs) have emerged in clinical applications due to their ability to differentiate into multi-lineage cell types such as chondrocytes, osteoblasts, and adipocytes(Murphy et al., 2013). In addition to their ability to self-renewal and less immunogenicity compared to other stem cells, hMSCs have been widely used. They also offer their financial advantages, availability and less ethical concerns compared to embryonic stem cells(Hsieh et al., 2013; Todeschi et al., 2015). For

these reasons, understanding and manipulating the metabolic regulations of hMSC can provide strategy for enhancing beneficial properties and safety to hMSC clinical applications. The present study aims to investigate the effects of succinate on hMSC mitochondrial dynamics and its related signaling pathways in hMSC function, along with clinical applications in skin wound healing *in vivo*.

MATERIALS AND METHODS

1. Materials

hMSCs were provided from the Medipost, Co. (Seoul, Korea). Fetal bovine serum was purchased from Bio Whittacker (Walkersville, MD, USA). The following antibodies were purchased: F-actin, phospho-PKC, phospho-DRP1, Gαq, Gαi and Gα12 antibodies (Cell Signaling Technology, Danvers, MA, USA); Cdc42, Rac1 and RhoA antibodies (BD Biosciences, Franklin Lakes, NJ, USA); DRP1, OPA1, Fis1, MFN2, p-ERK, p-JNK, ERK, JNK, GPR91, PKCδ, PKCε, PKCθ, PKCζ, profilin-1, phospho-cofilin1, cofilin1, β-actin and and β-tubulin antibodies (Santa Cruz Biotechnology, Paso Robles, CA, USC); COX IV antibody (Abcam, Cambridge, England); MFN2 antibody (Proteintech, Wuhan, China); Horseradish peroxidase (HRP)-conjugated goat anti-rabbit IgG (Jackson Immunoresearch, West Grove, PA, USA). Succinate, staurosporine,

NAC and mitomycin C were obtained from Sigma Chemical Company (St. Louis, MO, USA).

2. Cell culture

hMSC were cultured in α-minimum essential medium (Thermo, MA, USA) with 1% antibiotics (penicillin/streptomycin) and 10% FBS. Cells were grown at 37°C with 5% CO_2 in the incubator. When cells were grown 70% confluence, the medium was replace with serum-free medium excluding all supplements at 24 hr before experiments.

3. Mouse excisional wound splinting model

Eight-week-old male ICR mice were used. All animal procedures were performed with following the National Institutes of Health Guidelines for the Humane Treatment of Animals, with approval from the Institutional Animal Care and Use Committee of Seoul National University. Mice were anesthetized deeply with 3% isoflurane in a mixture of N_2O/O_2 gas (Suh and Han, 2015; Wang et al., 2013). To test the functional role of hMSCs pretreated with succinate, the mice were randomly divided into four groups: wild-

type mice that were treated with vehicle (group 1, n=6) or 50 μM succinate (group 2, n=6); hMSCs skin implantation group mice that were given succinate-stimulated hMSC (group 3, n=6) or that were given only hMSC (group 4, n=6). To determine the role of DRP1 in migration of hMSC to wound area for cutaneous regeneration, the mice were grouped into hMSCs transfected with *drp1* siRNA with (group 5, n=6) / without (group 6, n=6) succinate stimulation or *non-targeting* (*nt*) siRNA with (group 7, n=6) / without (group 8, n=6) succinate pretreatment. The back was shaved, sterilized with povidone iodine followed by 70% ethanol. The wound was created with using a 6 mm diameter sterile biopsy punch surgically. The hMSCs were pretreated with 50 μM succinate for 24 hr before the skin implantation. In the cell-treated group, 1×10^6 hMSC in 100 μl saline were injected into the dermis at three sites around the wound. After the cell transplantation, splints were placed around the wounds (with glue and several stitches) and then wounds were dressed with Tegaderm (3M, London, ON, Canada) sterile transparent dressing. Mice were placed in individual cages in a clean facility. Images of wound were acquired on day of 0, 5, 7 and 9 with a digital camera

system (40D, Canon, Tokyo, Japan) at the same distance (30 cm). At day 9, the wound tissues were embedded in OCT compound (Sakura, Finetek, Torrance, CA, USA) stored at −70℃, cut 6-㎛-thick frozen sections using cryosectioning machine and mounted on SuperFrost Plus slides (Thermo Fisher Scientific, Waltham, MA, USA) for haematoxylin and eosin (H&E) staining and immunohistochemistry.

4. Small interfering (si)RNA transfection

Cells were grown in 70% confluence and transfected for 24 hr with *drp1*, *Gαq*, *Gαi*, *Gα12*, *RhoA*, *Rac1*, and *Cdc42* siRNA (25 nM; Dharmacon, Lafayette, CO, USA) or *nt* siRNA as a negative control using Turbofect Transfection reagents (Thermo Fisher Scientific, Waltham, MA, USA) according to the manufacturer's instructions.

5. Wound-healing migration assay

Cells were seeded at $4 \times 10^3/\mu l$ in the both silicone reservoirs of 35-mm dishes (Ibidi, Martinsried, Germany). When cells were grown around 90% confluence, the medium was replace with serum-free medium. After 24 hr incubation, the silicone reservoirs

were carefully removed with sterile forceps for allowing the wound field. The cells were incubated another 24 hr with succinate and/or siRNA transfection and were incubated with phalloidin. Then the cells stained with phalloidin were visualized with an Olympus FluoView™ (Olympus, center Valley, PA, USA) 300 confocal microscope with 80× objective.

6. Oris™ cell migration assay

Cells were seeded at 3 × 10^3 cells/100 μL in Oris™ well (Platypus Technologies, Fitchburg, WI, USA) and were incubated for 24 hr to permit cell adhesion. When cells were grown 80% confluence, inserts were carefully removed, then cells were incubated with succinate (50 μM) and serum-free medium. After incubation, cells were stained with 5 μM calcein AM for 30 minutes and migrated cells were quantified by fluorescence signals measurement using Victor3 luminometer (PerkinElmer, Inc., Waltham, MA, USA) at excitation and emission wavelengths of 485nm and 515nm.

7. Reverse transcription polymerase chain reaction and real-time PCR

The hMSC RNA were extracted with the RNeasy Plus Mini Kit (QIAGEN, Valencia, CA, USA). Reverse transcription was performed with 3㎍ of RNA using a Maxime RT premix kit (iNtRON biotechnology, Seongnam, Korea). Real-time quantification of RNA targets was performed with Rotor-Gene 6000 thermal cycling system (Corbett Research, NSW, Australia) using QuantiTect SYBR green PCR kits (QIAGEN). The reaction mixture (20 ㎕) contained 200ng of RT products, 0.05㎍M of each primer, and appropriate amounts of enzymes and fluorescent dyes according to a manufacturer's instructions (Table 1). The fluorescent intensity was acquired during the extension step and melting curve analysis was performed to compare the expression of RNA targets.

Table 1. Sequences of primers used for RT-PCR

Gene name	Identification	Sequences (5' -3')
GPR91	Sense	CATTGTGACACGGCCTTTGG
	Antisense	TGTTTCACAAGCCCCTCACT
OPA1	Sense	GCAATGGGATGCAGCTATTT
	Antisense	GCAAGATAAGCTGGGTGCTC
MFN1	Sense	TGTTTTGGTCGCAAACTCTG
	Antisense	CTGTCTGCGTACGTCTTCCA
MFN2	Sense	TGTTGGCTCAGTGCTTCATC
	Antisense	AAGTCCCTCCTTGTCCCAGT
DRP1	Sense	CAGTGTGCCAAAGGCAGTAA
	Antisense	GATGAGTCTCCCGGATTTCA
Fis1	Sense	CTTGCTGTGTCCAAGTCCAA
	Antisense	GCTGAAGGACGAATCTCAGG

8. Western blot analysis

Harvested cells were lysed with RIPA lysis buffer for 30 min on ice. Protein concentration was determined by the Bradford method. Equal amounts of protein (20 μg) were resolved by 10% sodium dodecyl sulfate polyacrylamide gel electrophoresis (SDS-PAGE) and were transferred to polyvinylidene fluoride membranes. Membranes were incubated with indicated antibody followed by ECL treatment for detecting signals. The results were analyzed by optical density using Image J program.

9. Mitochondrial morphology analysis

According to the manufacturer's instructions, cells were cultured in confocal dish and incubated with Mitotracker Green FM (200 nM) for 30 min at 37 °C incubator. After incubation, cells were washed with pre-warmed media. Mitotracker Green-stained cells were visualized with confocal microscopy (× 400). Quantitative analysis of mitochondrial morphology was performed by using FIJI software. Mitochondrial morphology analyzed after thresholding. Individual mitochondria particles analyzed for circularity (Form factor = $(perimeter)^2$ / (4π * area)) and lengths ratio of major and minor axes. Form factor (FF) indicates mitochondrial length and branching and Aspect ratio (AR) imply length of the mitochondria. When FF and AR both increase, the mitochondria morphology becomes branched and elongated (Trudeau et al., 2011).

10. Measurement of calcium influx

Fluo-3AM which dissolved in dimethylsulfoxide were used to detect the intracellular Ca^{2+} levels. Cells in 35-mm confocal dish

were washed with PBS solution and incubated with a bath solution including 2 mM Fluo-3AM for 1 hr. After Fluo-3AM staining, Cells were washed twice with PBS solution and scanned with Olympus FluoView™ 300 confocal microscope with 300 × objective.

11. ATP assay

The intracellular ATP was measured with ENLITEN® ATP assay kit (Promega, Madison, WI, USA) according to manufacturer's instructions. Briefly, cells were boiled with lysis buffer at 100 °C for 5 min. Then the cell lysate centrifugated at 15,000rpm for 2 min. The extraction was collected and kept on ice. The same volume of the lysate and rL/L reagent incubated in the 96-well-plate. ATP concentration was normalized with ATP standard curve using ATP standard solution (10 μM).

12. Affinity precipitation

Activated RhoA, Rac1 and Cdc42 were detected with an affinity precipitation assay kits (EMD Millipore, Billerica, MA, USA) according to manufacturer's instructions. Lysed cells were incubated for 1 hr with agarose bead coupled with Rho-binding

domain of rhotekin (GST-Rhotekin-RBD) or Rac/Cdc42-binding domain (GST-PAK-PBD). After the incubation, agarose bead coupled with the lysate were eluted with 2× laemmli sample buffer and analyzed with western blot using RhoA, Rac1 and Cdc42 antibodies, respectively.

13. Co-immunoprecipitation (IP)

Cells lysed with the IP buffer (200 μg) were mixed with 10 μg of DRP1 antibody. The cell lysates were incubated for 4 hr with the antibody and then next 24 hr with the protein A/G PLUS-agarose immunoprecipitation reagent (Pierce, Rockford, IL, USA). After incubation, the beads were washed twice with IP buffer, and the bound proteins were eluted by sample buffer for 5 min. Samples were analyzed by western blotting with DRP1 and p-p38 antibodies.

14. Mitochondria membrane potential

The mitochondria membrane potential was evaluated with TMRE staining (abcam, Cambridge, U.K) according to the manufacturer's instructions. Cells were stained with TMRE (200 nM) with 5% CO_2 at 37 °C incubator for 30 min. CCCP (20 μM) were used as

negative control. After incubation, cells were washed with PBS solution. The intensity of TMRE staining was determined using flow cytometry and analyzed with CXP software (Beckman Coulter, Brea, CA, USA).

RESULTS

1. Succinate-pretreated hMSC promotes Skin Wound Healing in a Mouse Model

Because the GPR91 stimulating dose range by succinate differs from the cell types, I tested the enhancing effect of succinate on stem cell motility in a dose and time dependent manner. hMSCs were treated with various concentrations (0-500 μM) for 24 hr, and it was found that 50 to 500 μM of succinate increased stem cell migration (Fig. 1A). Stem cell motility was significantly increased after 24 hr succinate treatment (Fig. 1B). Additionally, mitomycin C (1 μg/mL) which inhibits the cell cycle did not affect succinate-induced stem cell motility suggesting the effect of succinate via GPR91 signaling independent of hMSC proliferation (Fig. 1C). To examine the effects of succinate on hMSC during skin wound healing, mice were divided into four groups: Vehicle, succinate, hMSC and hMSC with succinate, these were injected at

the wound areas separately. Succinate is thought to accelerate tissue regeneration with hMSC when exposed to wound sites separately. The sizes of the wound site were measured on days 0, 5, 7 and 9 until epithelialization was almost complete in the hMSC treatment group with succinate pretreatment. The wound area of the hMSC, succinate and succinate pretreated hMSC groups were significantly decreased compared to the vehicle. At day 9, I observed a significant wound size changes in the order of hMSC with succinate, hMSC alone, succinate and vehicle (Fig. 2A). In the wounds of hMSC and succinate alone groups, there were thin blood vessels and un-matured branches observed. However, in succinate-pre-stimulated hMSC-transplanted wound healing areas, thick blood vessels with finely branched vessels were observed in proximity to the wounds (Fig. 2B). A histological examination on day 9 showed that the wound sites of the succinate alone and hMSC alone groups were covered with epithelium, however, it was observed for the hMSC-treated group that the sites were filled with more granulation cells. Furthermore, succinate pretreated hMSC wound sites were completely re-epithelialized and covered with granulation tissue (Fig. 2C). Through these results, succinate

promotes tissue regeneration and accelerates the hMSC therapeutic function.

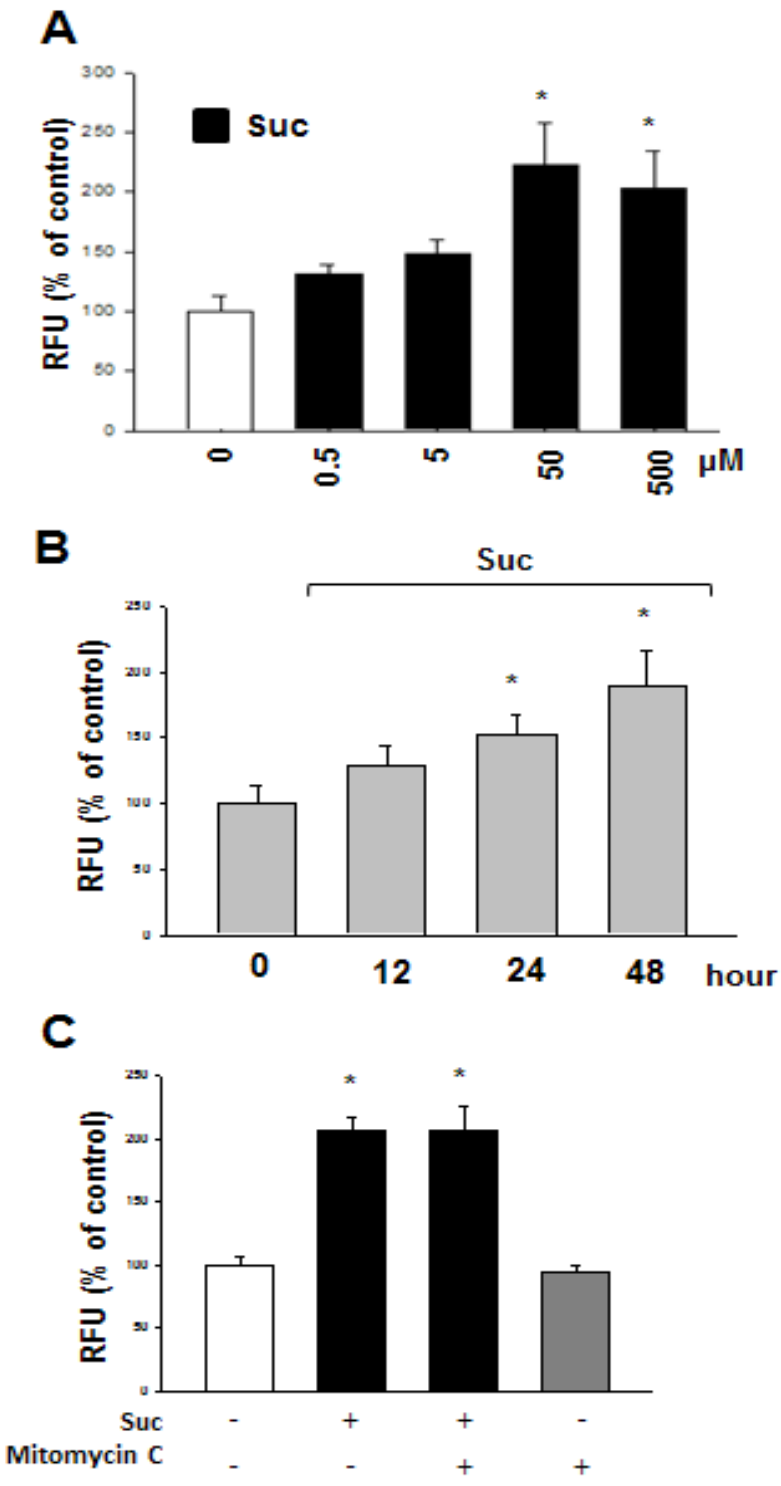
A
RFU (% of control)
Suc
300
250
200
150
100
50
0
*
*
0
0.5
5
50
500
μM
B
Suc
RFU (% of control)
*
*
0
12
24
48
hour
C
RFU (% of control)
*
*
Suc
Mitomycin C
-
+
+
-
-
-
+
+

Figure 1. Effect of succinate on hMSC migration (A) Dose responses of succinate for 24 hr in Oris™ cell migration assay were shown. Data represent mean ± S.E. n=4, $*p<0.05$ versus control. **(B)** Time responses of succinate in Oris™ cell migration assay were shown. Data represent the mean ± S.E. n=4. $* p<0.05$ versus control. **(C)** Effect of mitomycin C in succinate-induced hMSC migration. Cells treated with mitomycin C (1 μg/ml) for 90 min before succinate exposure. Data represent the mean ± S.E. n=4. $*p<0.01$ versus control.

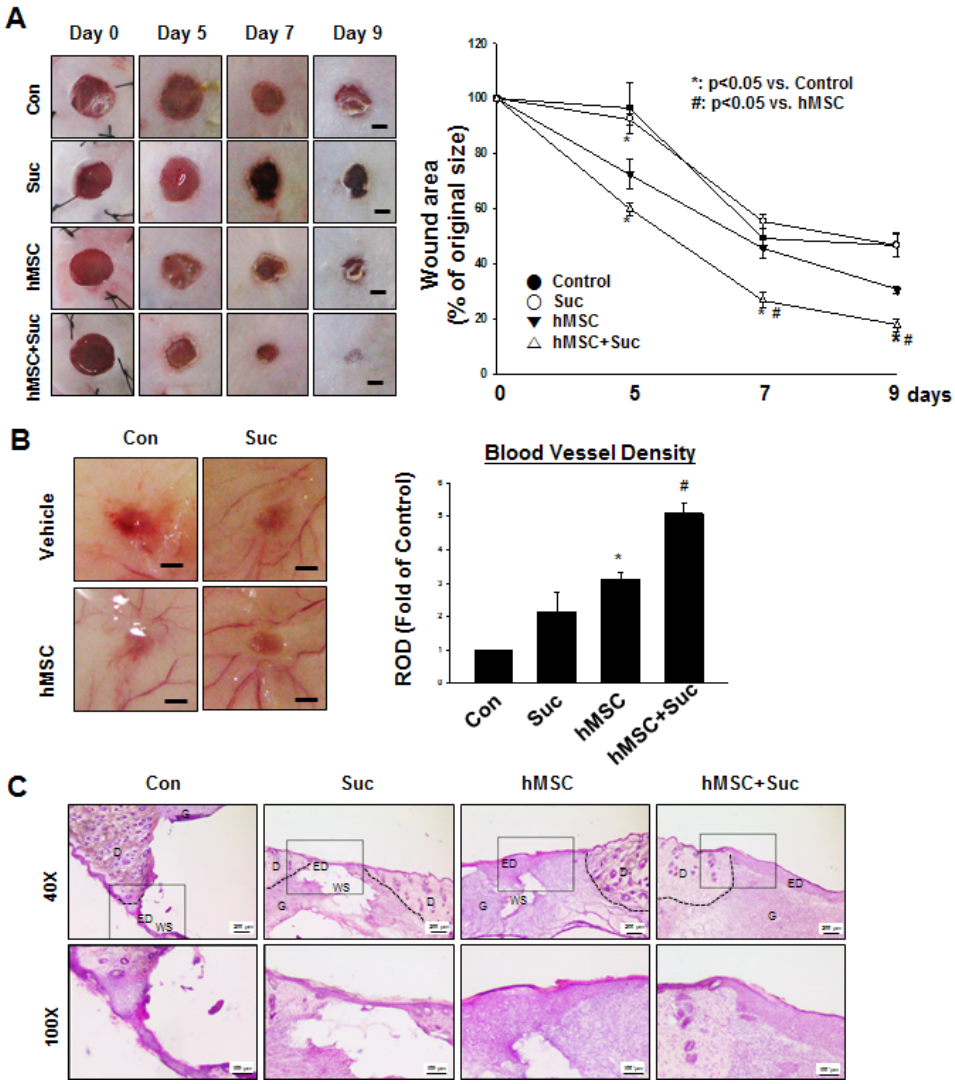
A
Day 0
Day 5
Day 7
Day 9
Con
Suc
hMSC
hMSC+Suc
*: p<0.05 vs. Control
#: p<0.05 vs. hMSC
Wound area
(% of original size)
Control
Suc
hMSC
hMSC+Suc
0
5
7
9 days
B
Con
Suc
Vehicle
hMSC
Blood Vessel Density
ROD (Fold of Control)
Con
Suc
hMSC
hMSC+Suc
C
Con
Suc
hMSC
hMSC+Suc
40X
100X
D
ED
WS
G

Figure 2. Effect of succinate on skin wound healing in vivo. (A) Mouse excisional wound splinting model were used to determining the effect of succinate on hMSC migration. Wounds were surgically made by 6-mm-diameter biopsy punch. Experimental animal were divided into four groups; control group (n=6), succinate group (n=6), hMSCs (1×10^6 cells) group (n=6), and succinate pre-stimulated hMSCs (1×10^6 cells) group (n=6). The representative images of skin wounds at days 0, 5, 7, and 9 are shown *(left panel)*. Determining wound healing by assessing the percentage of wound closures relative to original wound size. Data represent means ± S.E. n=6. $*p<0.05$ versus control, $^{\#}p<0.05$ versus hMSCs alone *(right panel)*. **(B)** The representative images of vascularity wound area at day were shown. Data represent means ± S.E. n=6. $*p<0.05$ versus control, $^{\#}p<0.05$ versus hMSCs alone. **(C)** Representative images of H&E tissue staining at day post wounding were shown. n=6. Scale bars=200 μm or 100 μm, magnification; ×40 or ×100 respectively.

2. Succinate Induces hMSC migration through GPR91-mediated PKC activation

To investigate the succinate-induced DRP1 phosphorylation signaling cascade, I hypothesized that succinate signaling initiates from GPR91 activation. After treatment with 50 μM of succinate, GPR91 mRNA and protein expression levels were analyzed with real-time PCR and western blotting. Both GPR91 mRNA and protein expression increased, suggesting that the GPR91 receptor exists in hMSC and involves in cell signaling (Fig. 3A, B). Succinate-induced hMSC migration into the wound area was inhibited by *gpr91* siRNA transfection (Fig. 3C). I carried out an Oris^{TM} migration assay to quantify the succinate-induced stem cell migration, and *gpr91* siRNA attenuated succinate- induced hMSC migration (Fig. 3D). Succinate led to the detachment of Gα_q, Gα_i, and Gα_{12} subunits from GPR91, and I need to determine which subunits played functional roles in succinate-induced hMSC migration (Fig. 4A). To verify which Gα subunits are involved in succinate-induced hMSC migration, *Gα subunit* siRNA transfection revealed that F-actin reorganized via Gα_q and Gα_{12} subunits (Fig. 4B). Consistently,

inhibition of $G\alpha_q$ and $G\alpha_{12}$ by siRNA transfection suppressed succinate-induced cell migration in both in vitro wound healing assay and Oris^{TM} cell migration assay (Figs. 4C, D). Succinate activated GPR91 to regulate PLC signaling and thus induce IP_3 accumulation, calcium mobilization and PKC activation (Mills and O'Neill). This motivated us to assess the level of PKC phosphorylation and the maximum phospho-pan PKC level was observed after 15 min of succinate treatment (Fig. 5A). To examine whether succinate increases Ca^{2+} influx further, Ca^{2+} was stained with Fluo-3AM. There was no change in the level of Ca^{2+} influx after succinate treatment while ionomycin (Ca^{2+} ionophore), as a positive control, drastically elevated Ca^{2+} influx (Fig. 5B). As Ca^{2+} was not involved in the phosphorylation of PKC, I examine Ca^{2+}-independent PKC expression in the Novel PKC (PKCδ, PKCε, and PKCθ) and the Atypical PKC (PKCζ) groups. Among Ca^{2+}-independent PKC samples, I observed only PKCζ translocated from cytosol to membrane after succinate treatment (Fig. 5C). The phosphorylation of PKC also depended on the regulation of $G\alpha_q$ and $G\alpha_{12}$ (Fig. 6A).

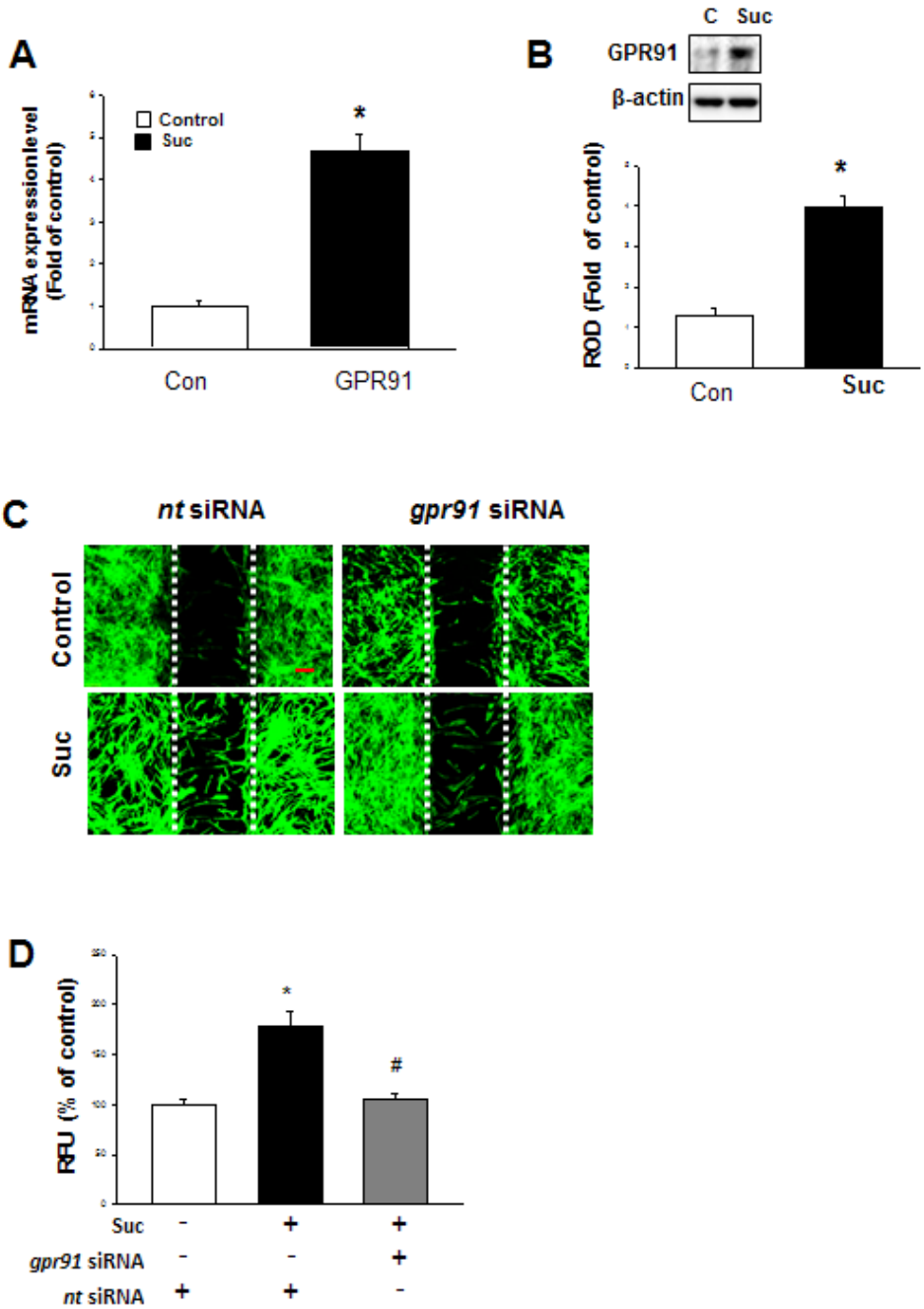
A
Control
Suc
mRNA expression level (Fold of control)
*
Con
GPR91
B
C
Suc
GPR91
β-actin
ROD (Fold of control)
*
Con
Suc
C
nt siRNA
gpr91 siRNA
Control
Suc
D
RFU (% of control)
*
#
Suc
gpr91 siRNA
nt siRNA

Figure 3. Involvements of GPR91 in succinate-induced hMSC migration. (A) hMSC were treated with succinate (10 μM) for 4 h and harvested for performing real-time PCR. The bars represents the mean ± S.E. n=3. *$p<0.05$* versus control. **(B)** Succinate was treated to hMSC for 4 hr. After incubation, cells were harvested for elucidating the existence of GPR91 in hMSC and increase of GPR91 in hMSC after succinate treatment. Anti-GPR91 antibody were used for western blotting. Error bars represent ± S.E. n=3. *$p<0.05$* versus control. **(C)** To determine whether GPR91 involved in the succinate-induced hMSC migration, *gpr91* siRNA were transfected. Cells were stained with phalloidin AlexaFlour 488 (Green) to identify the migrated cells. Scale bar=50 μm, magnification; × 80. **(D)** hMSC migration quantified with Oris™ cell migration assay was shown. Data indicate means ± S.E. n=4, *$p<0.05$* versus *nt* siRNA transfected cells, $^{\#}p<0.01$ versus succinate with *nt* siRNA transfected sample.

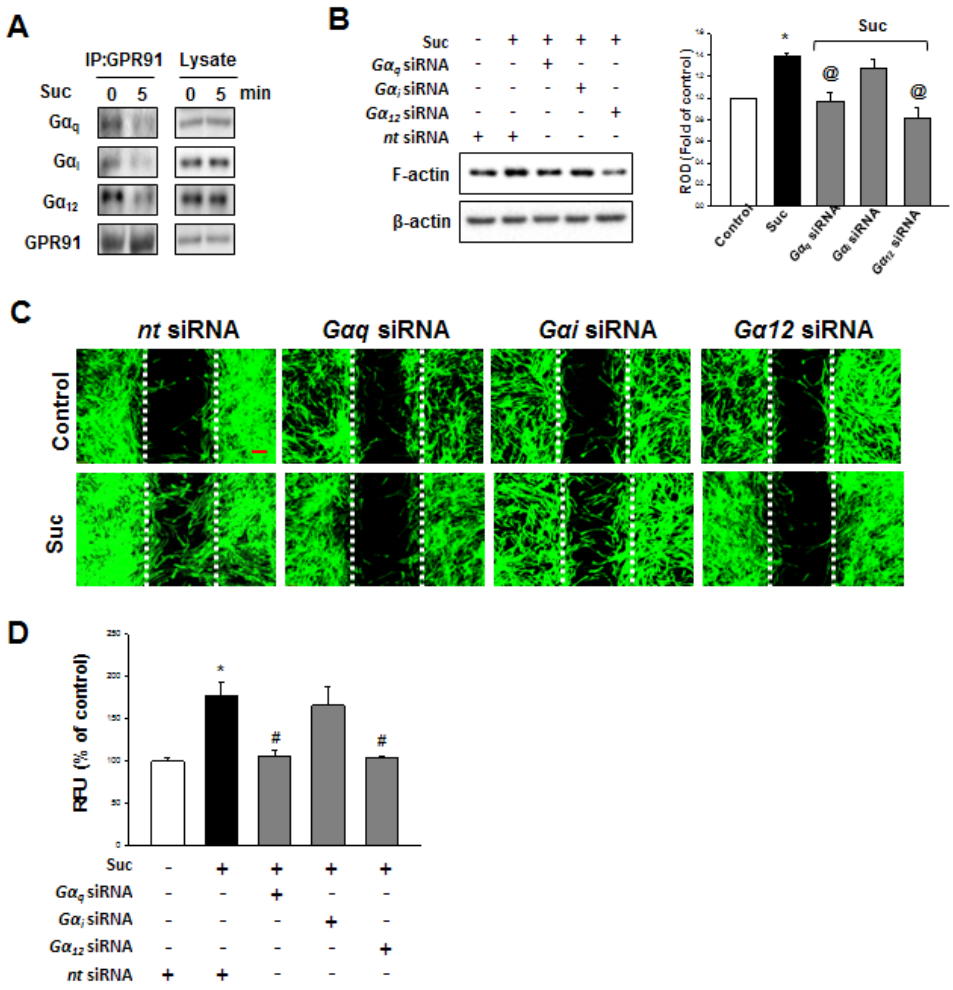
A
IP:GPR91
Lysate
Suc
0 5
0 5 min
Gαq
Gαi
Gα12
GPR91
B
Suc
Gαq siRNA
Gαi siRNA
Gα12 siRNA
nt siRNA
F-actin
β-actin
ROD (Fold of control)
Suc
Control
Suc
Gαq siRNA
Gαi siRNA
Gαi2 siRNA
C
nt siRNA
Gαq siRNA
Gαi siRNA
Gα12 siRNA
Control
Suc
D
RFU (% of control)
Suc
Gαq siRNA
Gαi siRNA
Gα12 siRNA
nt siRNA

Figure 4. Involvements of Gα complex in succinate-induced hMSC migration.

(A) hMSC were treated with succinate for 5 min. The total lysates were used for immunoprecipitation with anti-Gα_q, Gα_i, and Gα_{12} antibody. **(B)** *Gα_q*, *Gα_i*, and *Gα_{12}* siRNA transfected to hMSC prior to treatment of succinate for 24 hr. Cells were harvested for western bloting using anti-F-actin antibody. Error bars represent the mean ± S.E. n=3. $*p<0.01$ versus control, $^{@}p<0.05$ versus succinate treated cell. **(C)** Wound healing assay was performed to identify whether Gα_q and Gα_{12} were involved in succinate-induced cell migration. Scale bar=50 μm, magnification; × 80. **(D)** Gα_q and Gα_{12} mediated hMSC migration was quantified with Oris™ cell migration assay. Data represent means ± S.E. n=3, $*p<0.05$ versus control, $^{\#}p<0.01$ versus succinate alone.

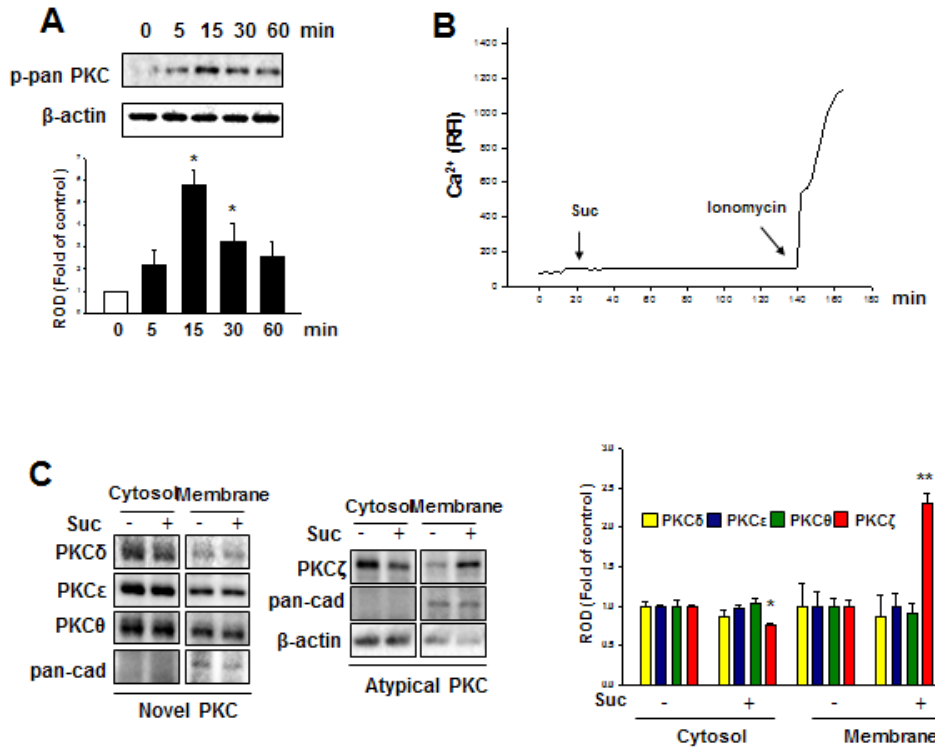
A
0 5 15 30 60 min
p-pan PKC
β-actin
ROD (Fold of control)
0 5 15 30 60 min
B
Ca2+ (RFI)
Suc
Ionomycin
min
C
Cytosol Membrane
Suc - + - +
PKCδ
PKCε
PKCθ
pan-cad
Novel PKC
Cytosol Membrane
Suc - + - +
PKCζ
pan-cad
β-actin
Atypical PKC
ROD (Fold of control)
PKCδ PKCε PKCθ PKCζ
Suc - + - +
Cytosol
Membrane

Figure 5. Effect of succinate on PKC phosphorylation.

(A) hMSC were treated with succinate for 0–60 min and cells analyzed by western blotting with anti-phospho PKC antibodies. Data represent means ± S.E. n=3, $*p<0.05$ versus control. **(B)** Cells were stained with Fluo-3AM for 1 hour and treated with succinate. Ionomycin (Ca^{2+} ionophore, 10 μM) were used as positive control. The changes of Fluo-3AM fluorescence were represented in relative fluorescence intensity (RFI, F/F_0%, arbitrary unit). **(C)** Cells were treated with succinate for 15 min and harvested for cytosolic/membrane fractionation. Translocation of PKC detected with novel PKC and atypical PKC antibodies. The pan-cadherin was used for plasma membrane control. Error bars represent means ± S.E. n=3. $**p<0.05$ versus cells without succinate treatment.

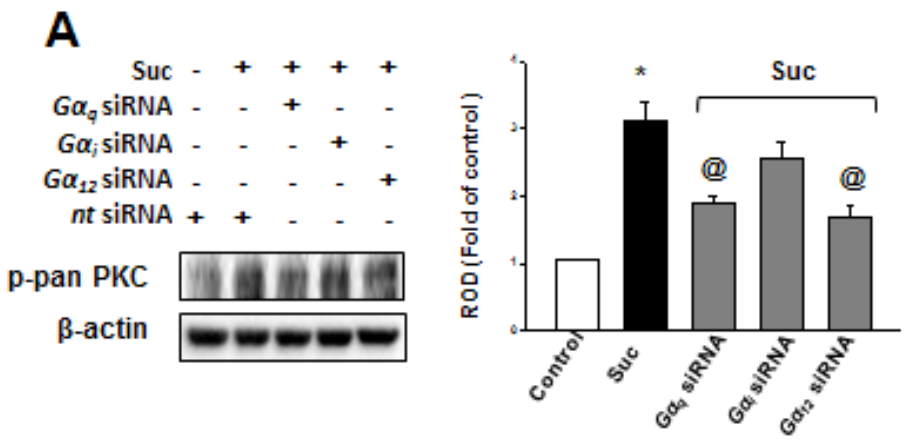
A
Suc - + + + +
Gαq siRNA - - + - -
Gαi siRNA - - - + -
Gα12 siRNA - - - - +
nt siRNA + + - - -
p-pan PKC
β-actin
ROD (Fold of control)
*
Suc
@
@
Control
Suc
Gαq siRNA
Gαi siRNA
Gα12 siRNA

Figure 6. Involvements of Gα complex in succinate-induced PKC activation.

(A) Cells were transfected with $G\alpha_q$, $G\alpha_i$, and $G\alpha_{12}$ siRNA for 24 hr before succinate treatment. hMSC was treated with succinate and harvested for western blot analysis with detecting p-pan PKC. Error bars represent the means ± S.E. n=3. $*p<0.05$ versus control, $^{@}p<0.05$ versus hMSC with succinate.

3. Succinate-Induced p38 Activation by PKC Involved in DRP1 phosphorylation

To investigate the succinate effect through GPR91, I examined GPR91 downstream kinase cascade and mitogen activated protein kinase (MAPK) signaling pathway. Among MAPKs, p38 activation increased in a time-dependent manner, especially 4 hr after succinate treatment (Fig. 7A). To examine whether PKC activation is involved in the succinate-induced p38 activation, I treated staurosporine (PKC inhibitor) which blocked the phosphorylation of p38 (Fig. 7B). To demonstrate the effect of succinate on mitochondrial dynamics related protein expression, I examined mRNA expression of succinate-induced mitochondrial dynamics related proteins. There is no significance change of mitochondrial dynamic related protein mRNA expression indicating that there is post translational modification on the protein (Fig. 8A, B). I demonstrated that succinate promoted a binding interaction between DRP1 and phospho-p38 compared to control (Fig. 9A). Consistently, confocal microscopy analysis revealed that DRP1 and p38 co-localizations were increased after succinate treatment to

hMSCs compared to the control (Fig. 9B). SB203580 (p38 inhibitor) blocked DRP1 phosphorylation at Ser 616 (Fig. 9C). The translocation of DRP1 from cytosol to mitochondria was also decreased by SB203580 in the hMSCs pretreated with succinate (Fig. 9D). To confirm that p38-induced DRP1 phosphorylation is related to hMSC migration, I observed that p38 inhibitor significantly blocked succinate-induced hMSC migration in Ibidi wound healing assay and Oris^{TM} migration assay (Figs. 10A, B). To elucidate the role of DRP1 in the succinate-induced hMSC cytoskeleton reorganization, *drp1* siRNA was transfected into hMSC, resulted hMSC failed to migrate (Figs. 11A-C).

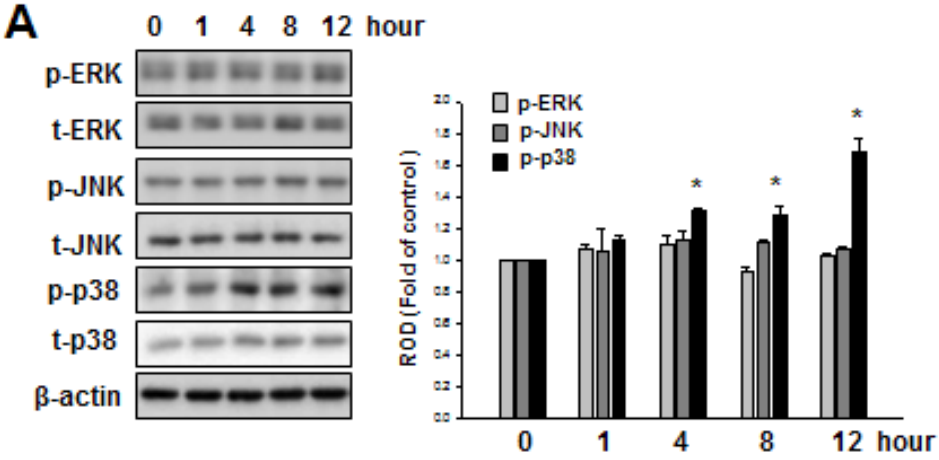
A
0 1 4 8 12 hour
p-ERK
t-ERK
p-JNK
t-JNK
p-p38
t-p38
β-actin
p-ERK
p-JNK
p-p38
ROD (Fold of control)
*
*
*
0 1 4 8 12 hour

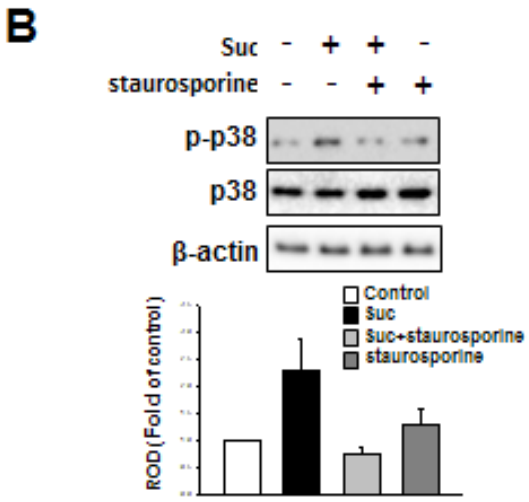
B
Suc - + + -
staurosporine - - + +
p-p38
p38
β-actin
Control
Suc
Suc+staurosporine
staurosporine
ROD (Fold of control)

Figure 7. Effect of succinate on p38 MAPK activation.

(A) hMSCs were treated with succinate for 0−12 hr and then harvested for western blotting to show the phosphorylation of MAPKs. The bars next part of the panel indicate the mean ± S.E. n=4, *$p<0.05$* versus 0 time. (B) Cells were treated with staurosporine (10 μM) for 30 min prior to succinate (50 μM) exposure for 12 hr. Phosphorylation of PKC in cells treated with succinate is shown. The bars below part of the panel indicate the mean ± S.E. n=3, *$p<0.05$ versus control.

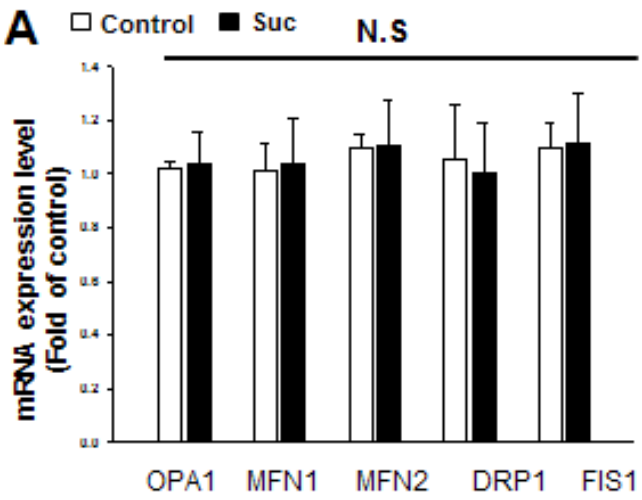
A
Control
Suc
N.S
mRNA expression level
(Fold of control)
OPA1
MFN1
MFN2
DRP1
FIS1

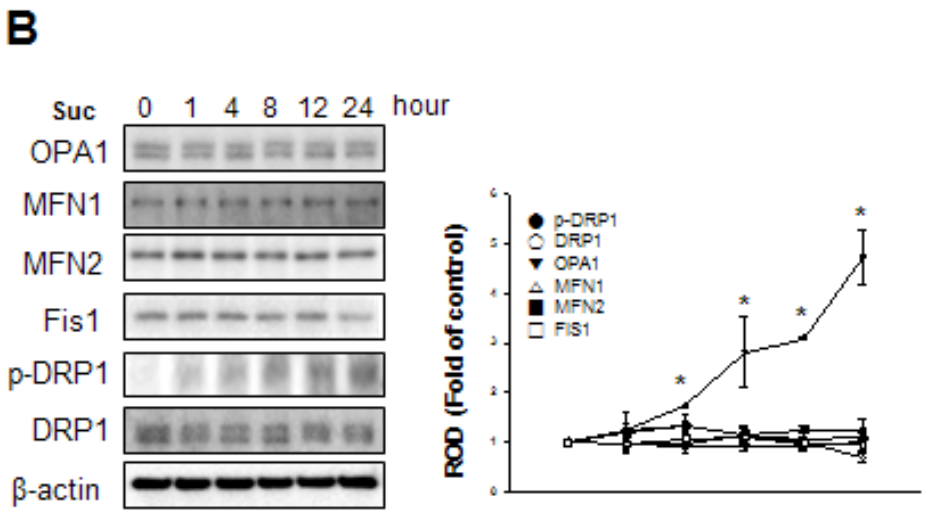
B
Suc
0 1 4 8 12 24 hour
OPA1
MFN1
MFN2
Fis1
p-DRP1
DRP1
β-actin
ROD (Fold of control)
p-DRP1
DRP1
OPA1
MFN1
MFN2
FIS1

Figure 8. Effect of succinate on mitochondrial dynamics-related proteins.

(A) Cells were pretreated with succinate for 12 h and then RNA extraction was carried out. Mitochondrial dynamics protein levels were determined with real-time PCR. The bars represents the mean ± S.E. n=4. N.S means 'not significant'.

(B) Succinate were treated for 0-24 h and cells were harvested for analyzing western blotting with anti-OPA1, MFN1/2, Fis1, p-DRP1, DRP1. The bars next to the panel indicated mean ± S.E for three experiments for each condition which is determined by densitometry relative to the loading control β-actin. *$p<0.05$ versus control.

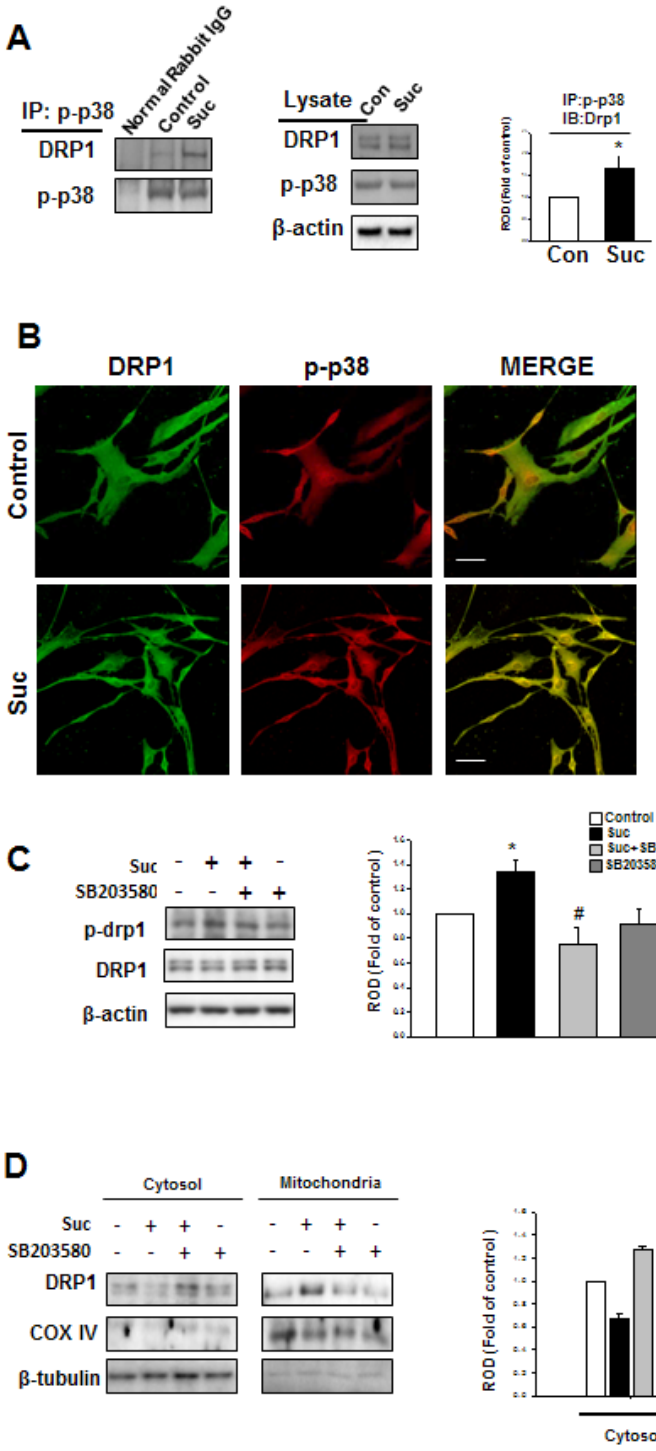
A
IP: p-p38
Normal Rabbit IgG
Control
Suc
DRP1
p-p38
Lysate
Con
Suc
DRP1
p-p38
β-actin
IP:p-p38
IB:Drp1
ROD (Fold of control)
Con
Suc
B
DRP1
p-p38
MERGE
Control
Suc
C
Suc
SB203580
p-drp1
DRP1
β-actin
ROD (Fold of control)
Control
Suc
Suc+SB203580
SB203580
D
Cytosol
Mitochondria
Suc
SB203580
DRP1
COX IV
β-tubulin
ROD (Fold of control)
Control
Suc
Suc+SB203580
SB203580
Cytosol
Mitochondria

Figure 9. Succinate-induced p38 MAPK activation regulates DRP1 phosphorylation.

(A) Cells treated with succinate for 12 hr and the total lysate were used for performing immunoprecipitation using normal rabbit IgG or p-p38 antibody to determine the protein binding. The bars below part of the panel represent the mean ± S.E. n=4, $*p<0.05$ versus control. **(B)** hMSC were treated with succinate (50 μM) for 12 hr. The co-localization of DRP1 (green) with p-p38 (red) was determined by confocal microscopy using immunofluorescence staining. Scale bars=50 μm, magnification; × 200 **(C)** hMSC pretreated with/without SB203580 (1 μM) for 30 min, and then exposed to succinate (50 μM) for 12 hr. The cell lysates were analyzed with western blotting, and detected with phospho-DRP1 Ser 616 antibody. The bars below part of panel denote mean ± S.E. n=3, $*p<0.05$ versus control, $^{\#}p<0.05$ versus succinate alone. **(D)** Cells were pretreated with SB203580 before succinate treatment for 12 hr and lysate was performed for mitochondrial fractionation. COX IV was used as mitochondria marker and β-tubulin was used for cytosolic marker. The bars below part of the panel indicate the mean ± S.E. n=3, $*p<0.05$ versus control, $^{\#}p<0.05$ versus succinate alone.

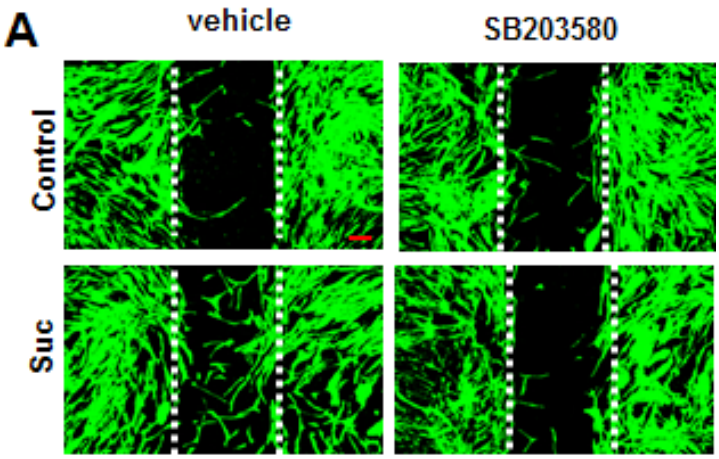
A
vehicle
SB203580
Control
Suc

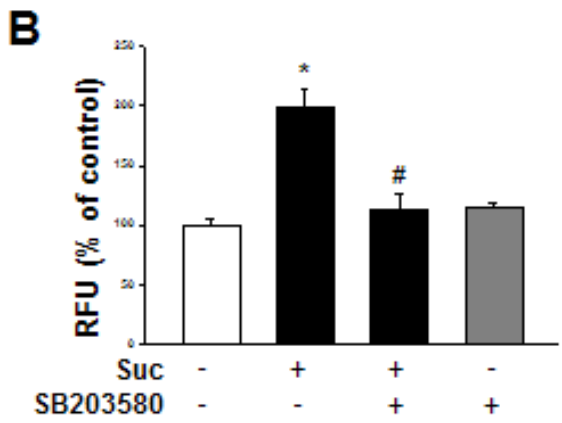
B
RFU (% of control)
*
#
Suc - + + -
SB203580 - - + +

Figure 10. Succinate-induced p38 activation involves in hMSC migration.

(A) Cells were pretreated with SB203580 prior to succinate treatment for 24 hr. After incubation, wound healing assay performed with phalloidin staining to identified migrating cell. Scale bar=50 μm, magnification; × 80. **(B)** Migrated cells were quantified with Oris™ migration assay. Data represent the mean ± S.E. n=3, $*p<0.05$ versus control, $^{\#}p<0.05$ versus succinate alone.

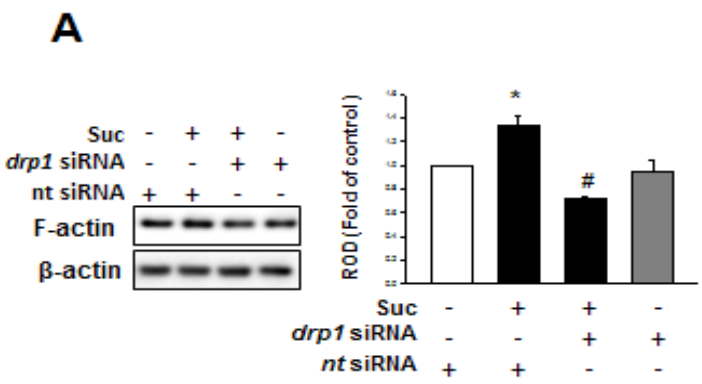
A
Suc - + + -
drp1 siRNA - - + +
nt siRNA + + - -
F-actin
β-actin
ROD (Fold of control)
*
#
Suc - + + -
drp1 siRNA - - + +
nt siRNA + + - -

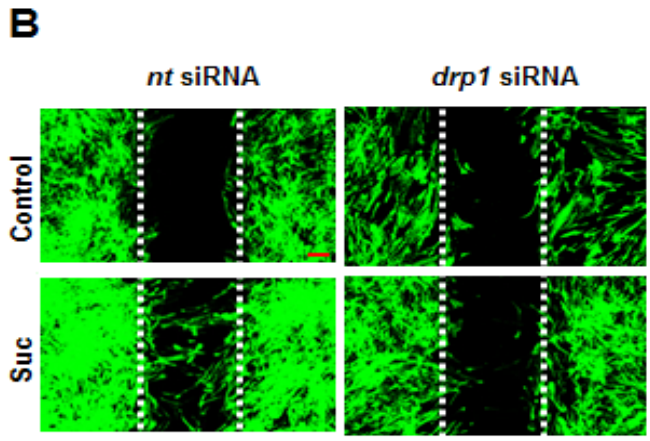
B
nt siRNA
drp1 siRNA
Control
Suc

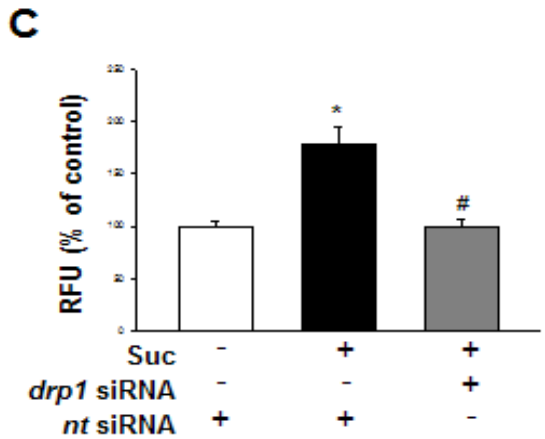
C
RFU (% of control)
*
#
Suc - + +
drp1 siRNA - - +
nt siRNA + + -

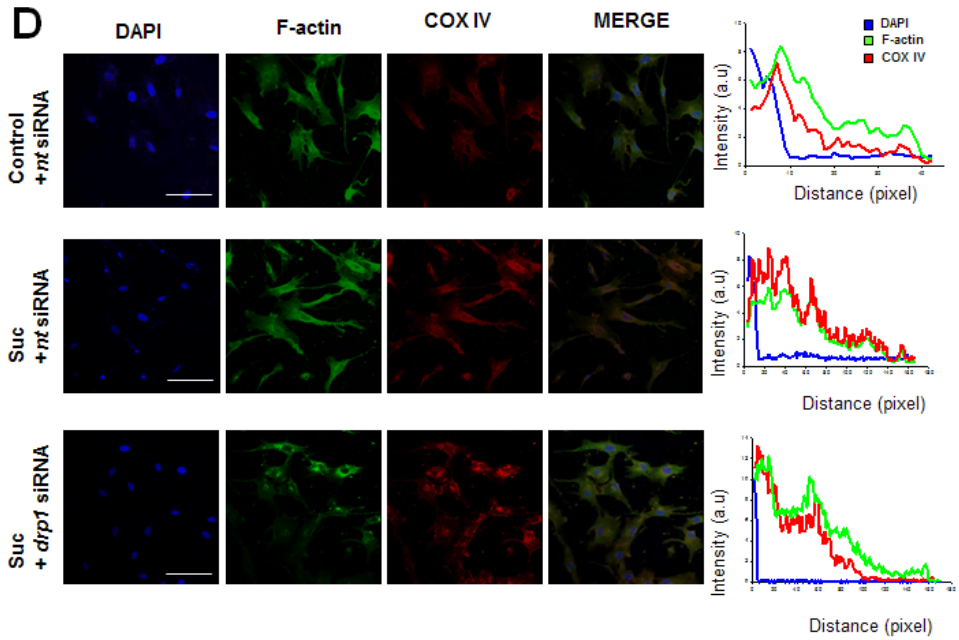
D
DAPI
F-actin
COX IV
MERGE
Control
+nt siRNA
Suc
+nt siRNA
Suc
+ drp1 siRNA
DAPI
F-actin
COX IV
Intensity (a.u)
Distance (pixel)
Intensity (a.u)
Distance (pixel)
Intensity (a.u)
Distance (pixel)

Figure 11. Effect of succinate-induced DRP1 phosphorylation on hMSC migration.

(A) *drp1* siRNA transfected in hMSC before succinate treatment for 24 h. After incubation with succinate, cells were analyzed by western blotting with anti-F-actin antibody. The bars next part of the panel represents the mean ± S.E. n=6, $*p<0.05$ versus *nt*siRNA, $^{\#}p<0.05$ versus succinate with *nt* siRNA. **(B)** Cells were cultured in ibidi confocal dish and transfected with *drp1* siRNA. Then cells were stained with phalloidin and observed with confocal microscopy. Scale bar=50 μm, magnification; × 80. **(C)** Migrated cells were quantified with Oris™ migration assay. Data represent the mean ± S.E. n=3, $*p<0.05$ versus control, $^{\#}p<0.05$ versus succinate with *nt* siRNA. **(D)** Succinate were treated for 24 h and cells were immunohistochemistry with F-actin (green), DAPI (blue) and COX IV (red) antibodies and the staining was observed with confocal microscopy. Representative confocal images were shown determined by at least 10 images from three independent experiments. The intensity graph next to confocal images indicates the distribution of F-actin (green) and COX IV (red) and observed that F-actin and COX IV co-localized with a great portion of intensity after succinate treatment, which attenuated the ratio of co-localization in *drp1* siRNA transfected hMSC. At least 20 to 30 cells were analyzed from three independent experiments. Scale bar = 100 μm. All distance and intensity measurements were determined with FIJI software.

4. DRP1-mediated Mitochondrial Fission Enhanced Mitochondrial Function

To determine whether mitochondrial dynamics is involved in succinate-induced hMSC migration, mitochondria were stained with MitoTracker Green and observed with confocal microscopy. Mitochondrial length was divided into three categories: >3 μm, 2-3 μm, and <2 μm. After succinate treatment, mitochondria were observed significantly fragmented compared to the control, and SB203580 treatment changed mitochondria morphology from fragmented to intermediate or elongated shape. In addition, the effects of succinate on mitochondrial morphology were analyzed with the AR and FF. After 24 hr succinate treatment, both AR and FF values were decreased by succinate treatment and the values were return to control levels after SB203680 treatment (Fig. 12A). I subsequently determined whether mitochondrial fission by succinate treatment affects the mitochondrial functions. After 24 hr succinate treatment, total ATP levels were significantly increased (612%) compared to the control (Fig. 13A). I confirmed that *drp1* siRNA transfection attenuated succinate-induced ATP levels to the

control levels (Fig. 13B). To determine whether succinate-induced ATP was related to mitochondrial ATP, I treated Oligomycin which inhibits mitochondrial F1F0-ATPase. Oligomycin downregulated succinate-induced ATP levels to the control level confirming that succinate-induced hMSC ATP enhancement was associated with mitochondrial ATP production (Fig. 13C). In addition, Oligomycin treatment attenuated succinate-induced F-actin formation (Fig. 13D). Succinate also increased mitochondrial membrane potential ($\Delta\psi_m$) consistent with ATP levels, and this was attenuated when cells were transfected with *drp1* siRNA (Fig. 14A).

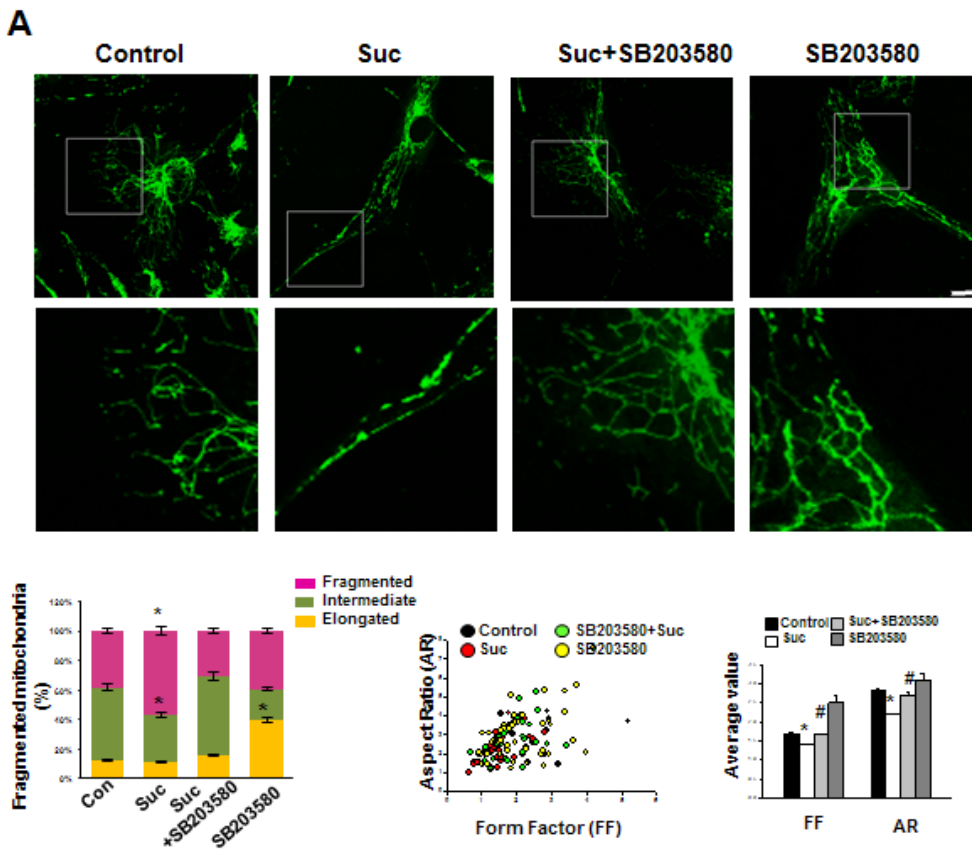
A
Control
Suc
Suc+SB203580
SB203580
Fragmented
Intermediate
Elongated
Fragmented mitochondria (%)
Con
Suc
Suc +SB203580
SB203580
Control
Suc
SB203580+Suc
SB203580
Aspect Ratio (AR)
Form Factor (FF)
Control
Suc
Suc+SB203580
SB203580
Average value
FF
AR

Figure 12. Effect of succinate on hMSC mitochondria morphology.

(A) hMSC was pre-treated with SB203580 and then exposed to succinate (50 μM) for 12 hr and then loaded with MitoTrakcer Green (200nM). Representative images were obtained by confocal microscopy. The individual mitochondrial length was assessed, classified into three different categories and quantified as percentage. Data denote mean ± S.E. n=10. Scale bar = 50 μm, magnification; × 200, *$p<0.05$* versus control.

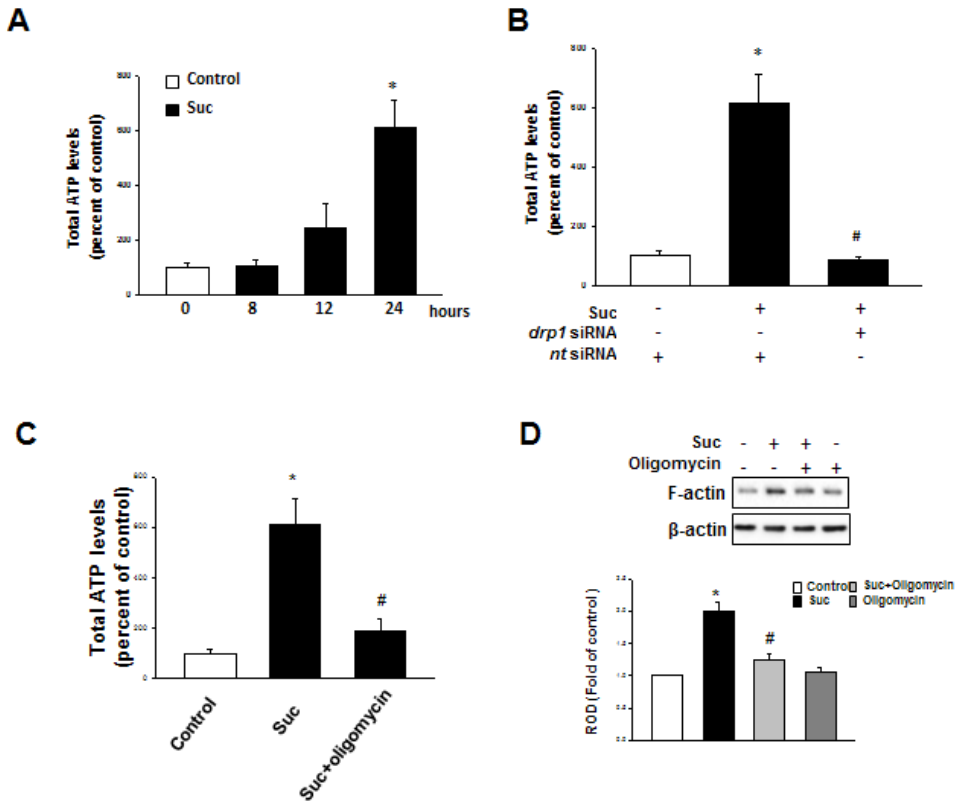
A
Control
Suc
Total ATP levels (percent of control)
0
8
12
24
hours
B
Total ATP levels (percent of control)
Suc
drp1 siRNA
nt siRNA
C
Total ATP levels (percent of control)
Control
Suc
Suc+oligomycin
D
Suc
Oligomycin
F-actin
β-actin
ROD (Fold of control)
Control
Suc
Suc+Oligomycin
Oligomycin

Figure 13. DRP1-mediated mitochondrial fission enhances mitochondrial ATP production.

(A) After incubation of hMSC with/without succinate (50 μM) for 0-24 hr, cells were lysed and reacted with ATP luciferase reagent. Then ATP levels were detected with luminometer. Data represents mean ± S.E. n=6. $*p<0.05$ versus control. **(B)** Cells were transfected with *drp1* siRNA prior to succinate (50 μM) treatment for 24 hr. Total cellular ATP levels were analyzed using ATP assay kit to detect luminescent ATP. Data represents mean ± S.E. n=6. $*p<0.05$ versus *nt* siRNA, $^{\#}p<0.05$ versus succinate with *nt* siRNA. **(C)** hMSCs were pretreated with oligomycin (1 μM) for 1 hr before succinate (50 μM) treatment for 24 hr. Total ATP levels were represents mean ± S.E. n=6. $*p<0.05$ versus control, $^{\#}p<0.05$ versus succinate. **(D)** hMSC were treated with Oligomycin (1 μM) for 1 hr prior to expose to succinate (50 μM) for 24 hr. Cells were harvested subjected to western blot and detected using F-actin antibody. Data represents ± S.E. n=3, $*p<0.05$ versus control, $^{\#}p<0.05$ versus succinate.

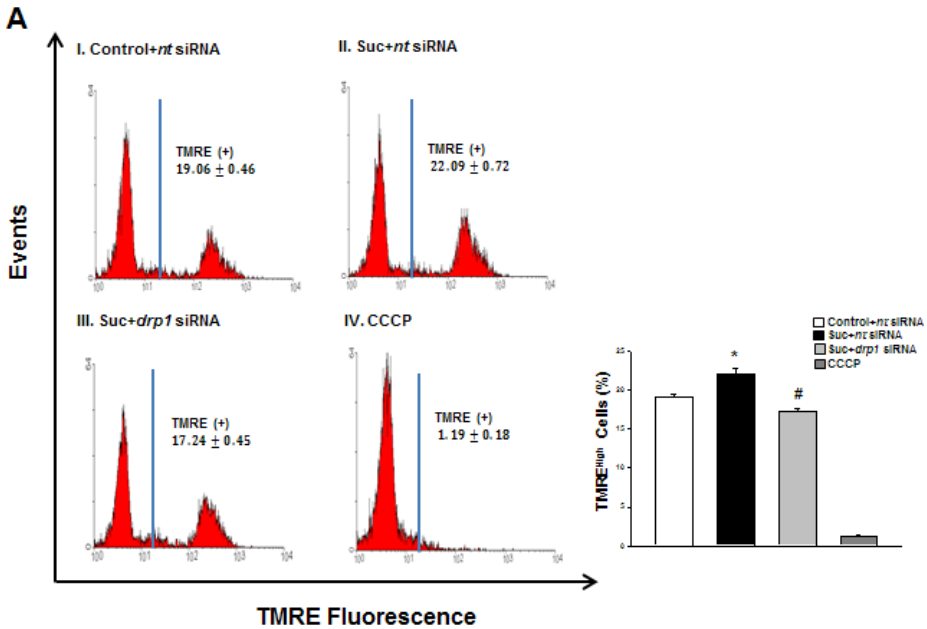

Figure 14. DRP1-mediated mitochondrial fission enhances mitochondria membrane potential.

(A) hMSCs were treated with succinate (50 μM) for the indicated time, and mitochondrial membrane potential was assessed by TMRE staining. Cells were transfected with *nt* siRNA or *drp1* siRNA and then treated with succinate for 24 hr. mitochondrial membrane potential stained with TMRE was measured using FACS analysis (total cell counts = 5000 cells). CCCP was used for negative control. The bars next to the panel represents ± S.E., n=3, $*p<0.05$ versus control + *nt* siRNA. $^{\#}p<0.05$ versus succinate + *nt* siRNA.

5. Succinate-Induced mtROS Enhanced F-actin Reorganization through Rho GTPase Activation

Increased mitochondrial respiration induces ROS production in various cells. Therefore, I confirmed succinate-induced ROS production using DCF-DA to detect the total cellular ROS level. After succinate treatment, ROS production was increased in a time-dependent manner (Fig. 15A). Generally, ROS was made from mitochondria and NADPH oxidase which can be inhibited by mitoTEMPO and VAS2870 respectively and N-acetylcysteine (NAC) can attenuate all two sources of ROS (Holmström and Finkel, 2014). My data showed succinate-induced ROS was inhibited by NAC and mitoTEMPO, indicating that the mitochondria were the major source of succinate-induced ROS production (Fig.15B). Additionally, *drp1* siRNA transfection attenuated mtROS, indicating ROS generated during DRP1-mediated mitochondrial fission (Fig. 15C). ROS is widely known to enhance cytoskeleton reorganization, accordingly, I investigated the effect of mtROS on the cytoskeletal dynamic-related small GTPases. Affinity precipitation for Rho GTPases revealed that the activities of RhoA, Rac1 and Cdc42 were

increased by succinate treatment in a time dependent manner (Fig. 16A). To determine whether mtROS affected to Rho GTPases, cells were treated with mitoTEMPO, resulting in downregulation of RhoA, Rac1 and cdc42 (Fig. 16B). Consistently, *RhoA, Rac1* and *Cdc42* siRNA significantly blocked the succinate-induced p-cofilin and profilin activation, which responsible for cell motility. (Fig. 16C). In addition, *RhoA, Rac1* and *Cdc42* siRNA transfection consequently suppressed hMSC migration to denuded area (Fig.17A) and in Oris™ migration assay (Fig. 17B). *RhoA GTPase* siRNA transfection significantly attenuated F-actin protein expression (Fig. 17C). These results demonstrated that increase of mtROS consequently enhance hMSC migration through Rho GTPase activation.

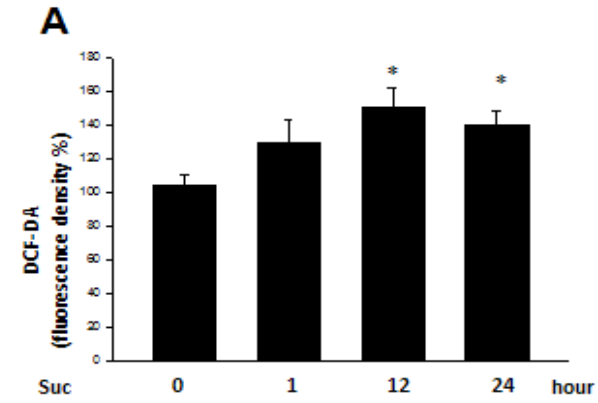
A
DCF-DA
(fluorescence density %)
180
160
140
120
100
80
60
40
20
0
*
*
Suc
0
1
12
24
hour

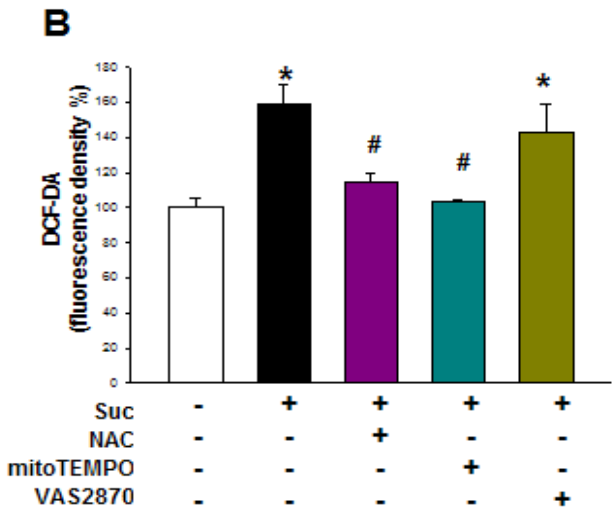
B
DCF-DA
(fluorescence density %)
180
160
140
120
100
80
60
40
20
0
*
#
#
*
Suc - + + + +
NAC - - + - -
mitoTEMPO - - - + -
VAS2870 - - - - +

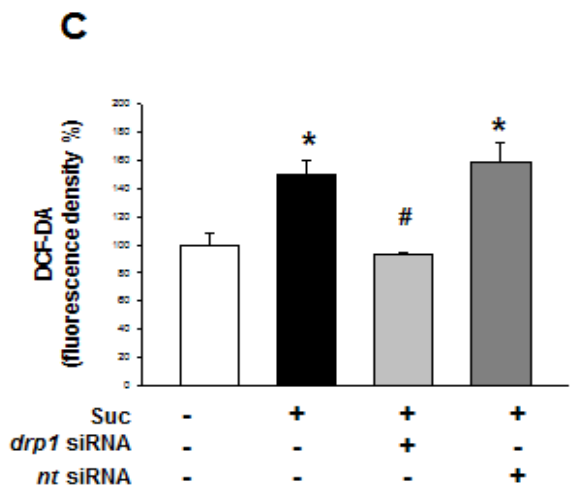
C
DCF-DA
(fluorescence density %)
*
#
*
Suc - + + +
drp1 siRNA - - + -
nt siRNA - - - +

Figure 15. Involvement of mtROS in succinate-induced DRP1 phosphorylation.

(A) hMSCs were treated with succinate (50 μM) for 0-24 hr and incubated with DCF-DA for 30 min to detect ROS using luminometer. $*p<0.01$ versus control. **(B)** hMSC was pretreated with NAC (1 mM), mitoTEMPO (20 μM) and VAS2870 (10 μM) for 30 min and incubated with succinate (50 μM) for 24 hr. Then hMSC was stained with DCF-DA and ROS levels were measured using luminometer. $*p<0.01$ versus control, $^{\#}p<0.05$ versus succinate. **(C)** hMSC was transfected with *drp1* siRNA and treated with succinate for 24 hr. The bars denotes ± S.E., n=6, $*p<0.05$ versus control, $^{\#}p<0.05$ versus succinate.

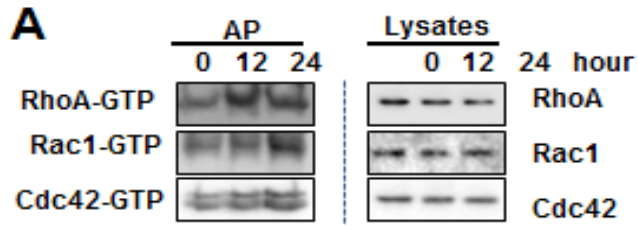
A
AP
Lysates
0 12 24
0 12 24 hour
RhoA-GTP
Rac1-GTP
Cdc42-GTP
RhoA
Rac1
Cdc42

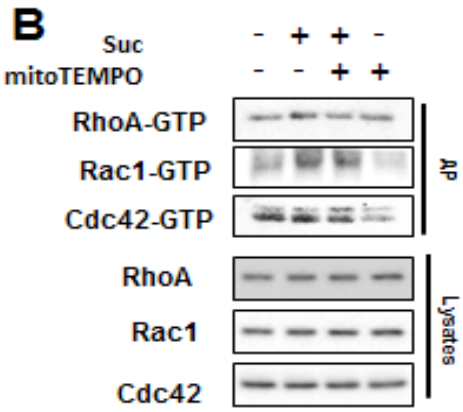
B
Suc
mitoTEMPO
RhoA-GTP
Rac1-GTP
Cdc42-GTP
RhoA
Rac1
Cdc42
AP
Lysates

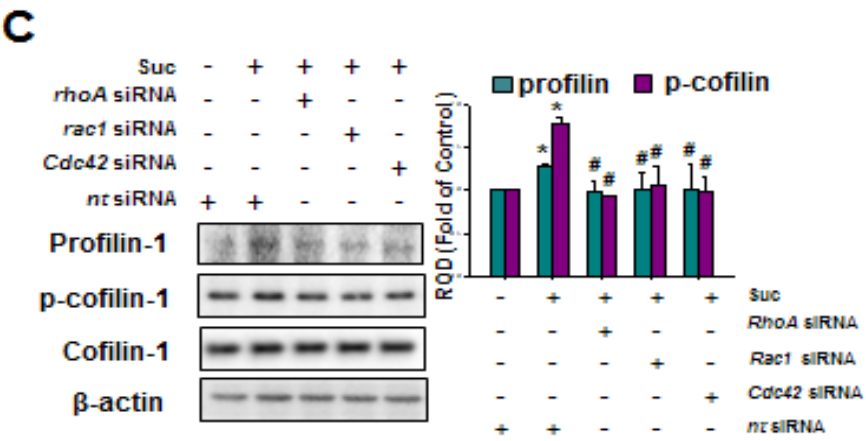
C
Suc
rhoA siRNA
rac1 siRNA
Cdc42 siRNA
nt siRNA
Profilin-1
p-cofilin-1
Cofilin-1
β-actin
profilin
p-cofilin
ROD (Fold of Control)
RhoA siRNA
Rac1 siRNA
Cdc42 siRNA
nt siRNA

Figure 16. Involvement of mtROS in succinate-induced F-actin formation..

(A) Cells were treated with succinate for 0-24 hr. AP were performed and Rho GTPases were detected with western blot analysis. **(B)** hMSCs treated with mitoTEMPO (20 μM) prior to expose to succinate for 24 hr. Then cells were analyzed with AP. **(C)** Cells were transfected *Rho GTPases* siRNA and then treated with succinate for 24 hr. Western blot performed to detect profilin, p-cofilin and cofilin protein expression. Error bars denote ± S.E. n=3, *$p<0.05$ versus control, #$p<0.05$ versus succinate alone.

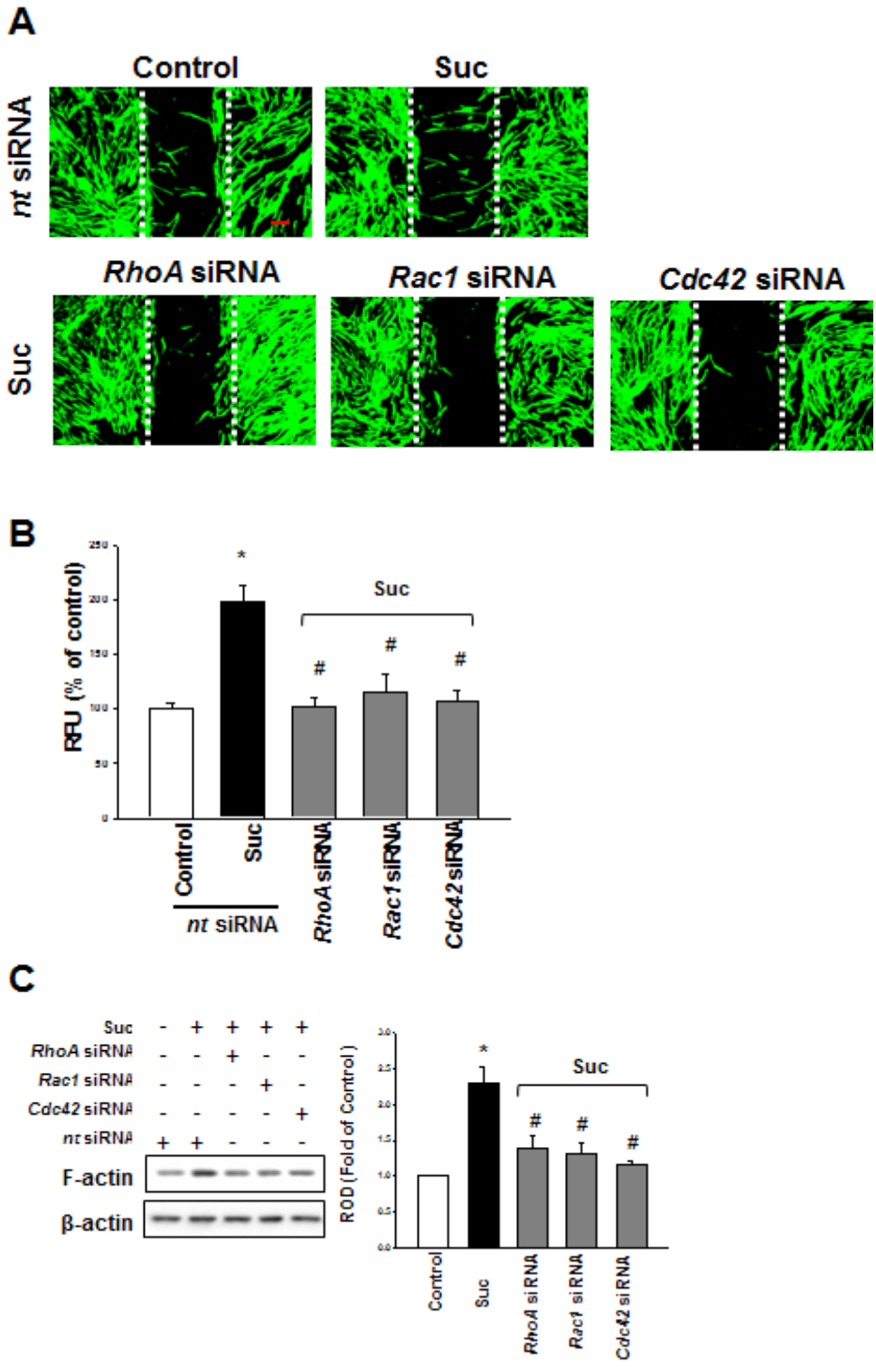
A
Control
Suc
nt siRNA
RhoA siRNA
Rac1 siRNA
Cdc42 siRNA
Suc
B
RFU (% of control)
Suc
Control
Suc
nt siRNA
RhoA siRNA
Rac1 siRNA
Cdc42 siRNA
C
Suc
RhoA siRNA
Rac1 siRNA
Cdc42 siRNA
nt siRNA
F-actin
β-actin
ROD (Fold of Control)
Suc
Control
Suc
RhoA siRNA
Rac1 siRNA
Cdc42 siRNA

Figure 17. Effect of succinate on hMSC F-actin formation.

(A) hMSC was cultured with ibidi dish and transfected with *RhoA, Rac1,*and *Cdc42* siRNA prior to 24 hr succinate treatment. And cells were stained with phalloidin and observed with confocal microscopy. (B) *Rho GTPases* siRNA-transfected cell was incubated with succinate for 24 hr and the hMSC migration were quantified with Oris™ migration assay. Data represent the mean ± S.E. n=4, $*p<0.05$ versus *nt* siRNA alone, $^{\#}p<0.05$ versus succinate with *nt* siRNA. (C) *Rho GTPases* siRNA transfected cells were treated for 24 hr and F-actin protein expression detected with western blotting. Error bars represent means ± S.E. n=3, $*p<0.05$ versus *nt* siRNA alone, $^{\#}p<0.05$ versus succinate with *nt* siRNA.

6. Succinate-Induced DRP1 Mediated Mitochondrial Fission Involved in Skin Regeneration Processes

To confirm the role of DRP1 on succinate-induced stem cell migration, hMSC was transfected with *drp1* siRNA or *nt* siRNA. As a results, hMSC with the vehicle and with the succinate were significantly decreased the size of the wound area on days 5 and 7. To verify the role of succinate during hMSC migration reciprocally DRP1-mediated mitochondrial fission, *drp1* siRNA was transfected into hMSCs showed considerably delayed cutaneous wound curing compared to the vehicle (Fig. 18A). Simultaneously, the effect of succinate pretreatment on the degree of vascularization was significantly attenuated in *drp1* siRNA transfected hMSCs, as observed in thin and unmatured blood vessel branches (Fig. 18B). A histological examination at day 9 showed that the wound healing was extremely delayed in hMSC+*drp1* siRNA treated mice group despite succinate treatment, whereas, hMSC+*nt* siRNA+succinate treatment led to almost completely recover with thick cornified epidermis (Fig. 18C). Concurrently, hMSC+succinate+*nt* siRNA treated mice group showed significantly increased numbers of cells

that migrated to the wound area for skin regeneration. However, the mice group treated with hMSC with *drp1* siRNA transfection showed failed stem cell transplantation with a failure to migrate to the wound site (Fig. 18D).

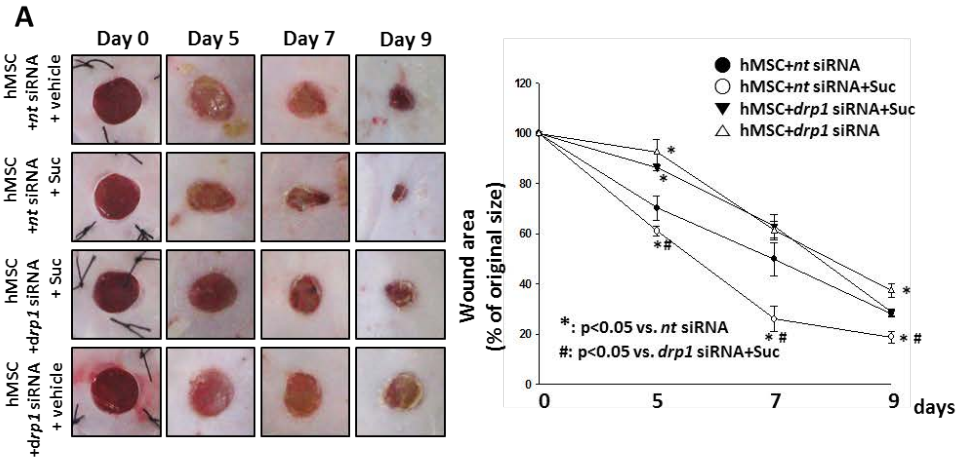
A
Day 0
Day 5
Day 7
Day 9
hMSC +nt siRNA + vehicle
hMSC +nt siRNA + Suc
hMSC +drp1 siRNA + Suc
hMSC +drp1 siRNA + vehicle
hMSC+nt siRNA
hMSC+nt siRNA+Suc
hMSC+drp1 siRNA+Suc
hMSC+drp1 siRNA
Wound area (% of original size)
*: p<0.05 vs. nt siRNA
#: p<0.05 vs. drp1 siRNA+Suc
days

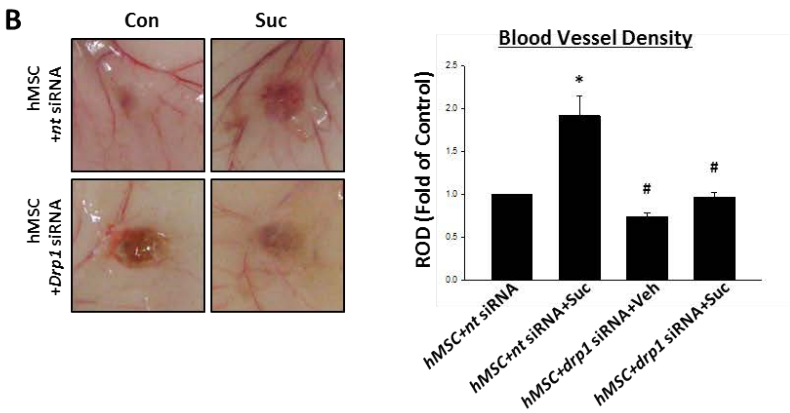
B
Con
Suc
hMSC +nt siRNA
hMSC +Drp1 siRNA
Blood Vessel Density
ROD (Fold of Control)
hMSC+nt siRNA
hMSC+nt siRNA+Suc
hMSC+drp1 siRNA+Veh
hMSC+drp1 siRNA+Suc

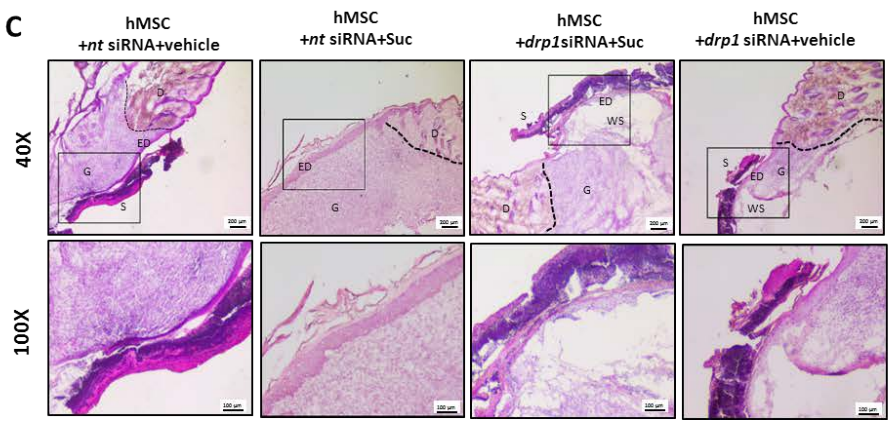
C
hMSC +nt siRNA+vehicle
hMSC +nt siRNA+Suc
hMSC +drp1siRNA+Suc
hMSC +drp1 siRNA+vehicle
40X
100X
D
ED
G
S
WS

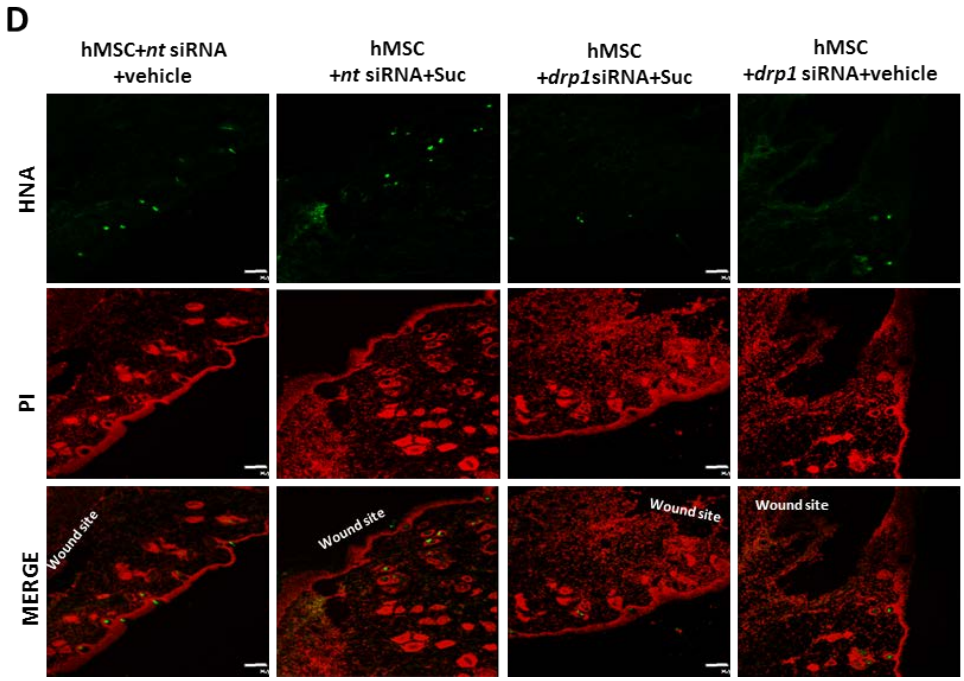

Figure 18. The role of DRP1 on skin wound healing in vivo. **(A)** Representative gross images of skin wound healing at day 0, 5, 7, and 9 are shown. Mouse skin wounds were surgically made by 6−mm−diameter biopsy punch and treated with hMSC + *nt* siRNA + vehicle, hMSC + *nt* siRNA + succinate, hMSC + *drp1* siRNA + succinate or hMSC + *drp1* siRNA + vehicle, respectively. *(left panel)* Determining wound healing by assessing the percentage of wound closures relative to original wound size. Data represent means ± S.E. n=6. $*p<0.05$ versus *nt* siRNA, $^{\#}p<0.05$ versus *drp1* siRNA + succinate *(right panel)*. **(B)** The quantified vascularity wound area at day 9 were shown. Data represent means ± S.E. n=6. $*p<0.05$ versus hMSC with *nt* siRNA, $^{\#}p<0.05$ versus hMSC with *nt* siRNA and succinate. **(C)** Representative wound tissues stained with H&E at day 9 were

shown. n=6, Scale bars=200 μm or 100 μm, magnification; ×40 or ×100 respectively. (D) Engraftment of hMSCs on wound at day 9 was observed by using confocal microscopy. Human nuclear antigen (HNA, green) was used for hMSC nuclear staining. Propidium iodide (PI, red) was used for nuclear counter staining, Scale bars=100 μm, magnification; × 100.

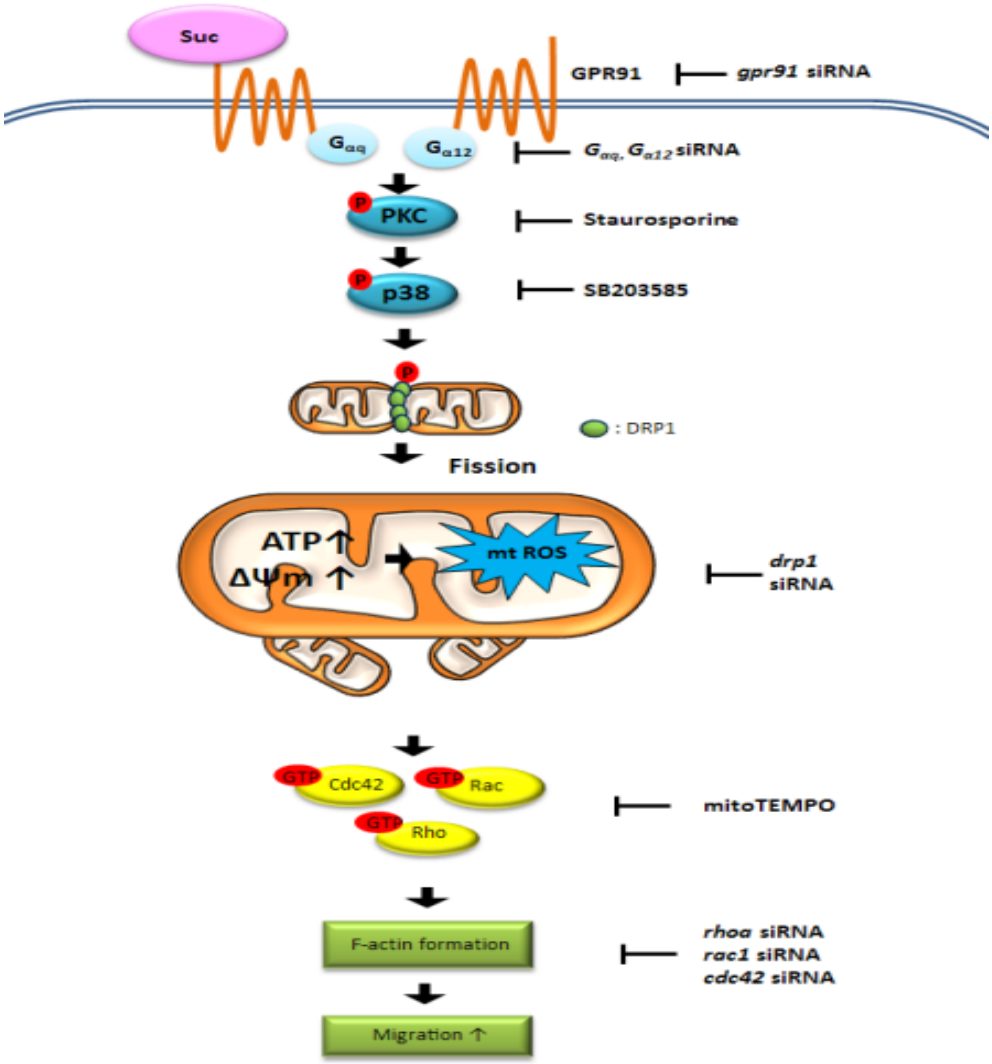

Figure 19. Schematic diagram for the effect of succinate on hMSC migration through mitochondrial fission.

DISCUSSION

In present study, I demonstrated that underlying molecular mechanism of mitochondrial fission by succinate is closely associated with hMSC motility and that pretreatment of succinate enhanced hMSC migration in skin wound healing in vivo. Succinate is a charged molecule, therefore it binds to its specific receptor, GPR91, under a physiological pH (He et al., 2004). The physiological response to succinate varies depending on its concentration. In previous reports, a high succinate concentration (10 mM) with prolonged incubation induced cell apoptosis, whereas, a succinate concentration at the physiological level played an essential role in hepatic stellate cell (HSC) regeneration through the GPR91 signaling pathway (Hamel et al., 2014; Li et al., 2015), indicating that ex-vivo stimulation with hMSC can be a target to promote the wound healing process. I also confirmed the importance of an adequate succinate concentration (50 μM) and time (24 h) on

the enhancement of hMSC motility at physiological level. GPR91 interacts with various G proteins, including $G\alpha_i$ or $G\alpha_q$ and triggers diverse pathways for each specific cell type (Rubic et al., 2008), accordingly which G protein is interacted with GPR91 in hMSC should be elucidated. I clearly demonstrated that GPR91 activation occurred through $G\alpha_q$ and $G\alpha_{12}$. An earlier study showed that $G\alpha_q$ and $G\alpha_{12}$ double-knock out mouse embryos died in utero, although an individually deficient mouse survived, suggesting that $G\alpha_q$ and $G\alpha_{12}$ play pivotal roles in cell functions via their interactive actions (Gao and Kapusta, 2015; Gu et al., 2002). GPR91 becomes activated depending on $G\alpha_i$ through Ca^{2+} upregulation, which consequently activates PLC to activate PKC in HEK293 cells (Sundström et al., 2013). In contrast, in my study, succinate did not alter Ca^{2+} mobilization and $G\alpha_q$ and $G\alpha_{12}$ siRNA transfection attenuates the phosphorylation of PKC. Among the novel and atypical types of PKC which are unassociated with intracellular Ca^{2+} signaling, PKCζ was translocated from the cytosol to the membrane by succinate. $G\alpha_q$ has been identified as a scaffold protein that directly interacts with close proximity to PKCζ activation to transduce extracellular signaling via ERK5 activation

(Garcia-Hoz et al., 2010). Furthermore, stromal cell-derived factor-1 (SDF-1) induces hMSC migration through p38 MAPK, indicating that MAPK can be a targeted downstream effector of PKCζ (Ryu et al., 2010). Moreover, GPR91 activation induced VEGF release mediated p38 MAPK signaling in RGC-5 cells (Hu et al., 2015). Consistent with these results, my data showed that staurosporine significantly decreased p38 MAPK phosphorylation suggesting that succinate induces p38 MAPK via Gα_q and Gα_{12} dependent PKC activation.

It has been reported that mitochondrial dynamics can tightly regulate cellular bioenergetic roles and homeostasis (Benard et al., 2011; Nasrallah and Horvath, 2014). This prompted us to investigate the relevance of succinate and mitochondrial dynamics on hMSC migration. The regulation of mitochondrial morphology is associated with mitochondrial functions and is tightly regulated by the mitochondrial dynamics proteins . The mitochondrial dynamics protein expression level and post-translational modifications control the associated protein activities (Wang et al., 2012). My study demonstrated that there were no significance alterations of the mitochondrial dynamics protein mRNA expression levels, except

for the phosphorylation of the DRP1 protein at the Ser616 site (Figure 8). In addition, succinate-induced p38 MAPK phosphorylation directly activated DRP1, consequently induced mitochondrial fragmentation. Mitochondrial fission can be a double-edged sword, when it occurs in a pathophysiological condition, resulting in energy production depletion and mitochondrial depolarization and causing mitochondria to undergo autophagic degradation (Jheng et al., 2012; Kim et al., 2016). On the other hand, in a physiological condition, fragmented mitochondria are distributed equitably in proliferative cells and are essential to maintain cell polarity and enhance mitochondrial respiration during the neuronal axon formation process (Archer, 2013; Cho et al., 2013; Taguchi et al., 2007). Although several studies have shown that mitochondrial fission protein DRP1 plays roles in cell migration by increasing of mitochondrial respiration, the detailed molecular mechanism acting under mitochondrial fission-mediated migration has yet to be elucidated. This is the first report finding that succinate-mediated mitochondrial fission regulates the functional migrated activities of hMSC. My study clearly showed that DRP1-mediated mitochondrial fragmentation by succinate is vital to

enhance cellular respiration, indicating that succinate-induced mitochondrial morphology alteration can be a target to regulate hMSC physiological cellular function. My study clearly demonstrated that mitochondrial ATP is an important part of the physiology of stem cells. I confirmed that mitochondria fission resulted in an increase in the number of mitochondria with redistribution in the direction of hMSC migration, indicating lamellipodia and filopodia (Figure 9), and hypothesized that mitochondrial redistribution plays important roles in transporting other organelles which can maintain cellular homeostasis and supply energy to where it is needed (Kaksonen et al., 2006).

It has also been reported that a high glucose level makes mitochondria fragments which are necessary to increase respiration, consequently inducing ROS production (Yu et al., 2006). However, the interaction between succinate and the mitochondrial functions during stem cell migration has not been investigated extensively. Mild ROS have been emerged as a signaling molecule that regulates a broad range of cellular functions, and my study showed that ROS affected by succinate at physiological levels regulates hMSC migration as a signaling molecule (Panieri and Santoro, 2015).

Although ROS is widely known rapidly to induce a cellular response, previous studies have demonstrated that sustained ROS generation is involved in the wound healing process in zebra fish, and further study must be done in the area of stem cell physiology (Gauron et al., 2013). My work showed that sustained mtROS can be a key molecule to regulate hMSC behavior. There have been several reports that mtROS can induce cell migration via various forms of downstream signaling in endothelial cells (Wang et al., 2011) and that mutations in mitochondrial DNA (mtDNA) induce the overproduction of mtROS resulting in tumor cell metastasis together with cell migration (Ishikawa et al., 2008). ROS can activate the Rho small GTPase family during cell migration. There is evidence that ROS generated by NOX directly regulate cytoskeleton organization in relation to cofilin activity, a major regulator of actin polymerization (Bernstein and Bamburg, 2010). It is not clear whether succinate influences additional cytoskeleton reorganization such as a loss of cell adhesion or other independent cellular signaling activities. My data, however, clearly showed that mtROS activated Rho small GTPase activity which regulates profilin and cofilin activity in the actin filament assembly. My study also

suggests that mitochondrial fission, mtROS and cell migration are functionally linked, therefore, further study is required to elucidate the molecular mechanisms associated with mitochondrial dynamics during the regulation of stem cell behavior and wound healing more precisely.

To the best my knowledge, this is the first reports that mitochondrial dynamics under succinate-induced GPR91 activation regulates the functional migrated activities of hMSC. Interestingly, my in vivo data clearly showed that DRP1 plays a critical role in not only GPR91-mediated hMSC migration but also that hMSC's clinical effect on skin regeneration. Contrary to my expectations, succinate alone treated mice group showed no positive effects on accelerating vascularity, indicating that succinate may have therapeutic potential only when treated with hMSCs. My in vivo data suggests that the TCA cycle metabolite is a very novel bioactive molecule to modulate hMSC mechanistic function through regulating stem cell mitochondrial functions in regenerative medicine in less time and at a lower cost. Further study may need to elucidate the full potential of succinate in stem cell-based therapy, although my results showed the effect, and have to be shown the potential of

developing new treatment designs involving for targeting migration aspects of stem cells based upon my study.

References

Archer, S.L. (2013). Mitochondrial dynamics—mitochondrial fission and fusion in human diseases. New England Journal of Medicine *369*, 2236–2251.

Ariza, A.C., Deen, P.M., and Robben, J.H. (2012). The succinate receptor as a novel therapeutic target for oxidative and metabolic stress–related conditions. Frontiers in Endocrinology *3*, 22.

Benard, G., Bellance, N., Jose, C., and Rossignol, R. (2011). Relationships Between Mitochondrial Dynamics and Bioenergetics. Mitochondrial dynamics and Neurodegeneration. Springer Netherlands, 47–68.

Bernstein, B.W., and Bamburg, J.R. (2010). ADF/cofilin: a functional node in cell biology. Trends in Cell Biology *20*, 187–195.

Buravkova, L.B., Andreeva, E.R., Gogvadze, V., and Zhivotovsky, B. (2014). Mesenchymal stem cells and hypoxia: where are we?. Mitochondrion *19 Pt A*, 105–112.

Carey, B.W., Finley, L.W., Cross, J.R., Allis, C.D., and Thompson, C.B. (2015). Intracellular alpha–ketoglutarate maintains the pluripotency of embryonic stem cells. Nature *518*, 413–416.

Cherry, C., Thompson, B., Saptarshi, N., Wu, J., and Hoh, J. (2016). 2016: A 'mitochondria' odyssey. Trends in Molecular Medicine *22*, 391-403.

Cho, B., Choi, S.Y., Cho, H.M., Kim, H.J., and Sun, W. (2013). Physiological and pathological significance of dynamin-related protein 1 (Drp1)-dependent mitochondrial fission in the nervous system. Experimental Neurobiology *22*, 149-157.

Chouchani, E.T., Pell, V.R., Gaude, E., Aksentijevic, D., Sundier, S.Y., Robb, E.L., Logan, A., Nadtochiy, S.M., Ord, E.N.J., Smith, A.C., *et al.* (2014). Ischaemic accumulation of succinate controls reperfusion injury through mitochondrial ROS. Nature *515*, 431-435.

Ding, D.-C., Chang, Y.-H., Shyu, W.-C., and Lin, S.-Z. (2015). Human umbilical cord mesenchymal stem cells: a new era for stem cell therapy. Cell transplantation *24*, 339-347.

Ejtehadifar, M., Shamsasenjan, K., Movassaghpour, A., Akbarzadehlaleh, P., Dehdilani, N., Abbasi, P., Molaeipour, Z., and Saleh, M. (2015). The Effect of Hypoxia on Mesenchymal Stem Cell Biology. Advanced Pharmaceutical Bulletin *5*, 141-149.

Folmes, C.D.L., and Terzic, A. (2016). Energy metabolism in the acquisition and maintenance of stemness. Seminars in Cell & Developmental Biology *52*, 68-75.

Gao, J., and Kapusta, D. (2015). Contribution of Brain Gαq and Gα12 Protein Pathways in Mediating Angiotensin II (Ang II) Dependent Hypertension. The FASEB Journal *29*, 968.921.

Garcia-Hoz, C., Sanchez-Fernandez, G., Diaz-Meco, M.T., Moscat, J., Mayor, F., and Ribas, C. (2010). G alpha(q) acts as an adaptor protein in protein kinase C zeta (PKCzeta)-mediated ERK5 activation by G protein-coupled receptors (GPCR). The Journal of Biological Chemistry *285*, 13480-13489.

Gauron, C., Rampon, C., Bouzaffour, M., Ipendey, E., Teillon, J., Volovitch, M., and Vriz, S. (2013). Sustained production of ROS triggers compensatory proliferation and is required for regeneration to proceed. Scientific Reports *3*, 2084.

Gu, J.L., Muller, S., Mancino, V., Offermanns, S., and Simon, M.I. (2002). Interaction of G alpha(12) with G alpha(13) and G alpha(q) signaling pathways. Proceedings of the National Academy of Sciences of the United States of America *99*, 9352-9357.

Haas, R., Cucchi, D., Smith, J., Pucino, V., Macdougall, C.E., and Mauro, C. Intermediates of Metabolism: From Bystanders to Signalling Molecules. Trends in Biochemical Sciences *41*, 460-471.

Hamel, D., Sanchez, M., Duhamel, F., Roy, O., Honore, J.C., Noueihed, B., Zhou, T., Nadeau-Vallee, M., Hou, X., Lavoie, J.C., *et al.* (2014). G-protein-coupled receptor 91 and succinate are key contributors in neonatal postcerebral hypoxia-ischemia recovery. Arteriosclerosis, Thrombosis, and Vascular Biology *34*, 285-293.

Citric acid cycle intermediates as ligands for orphan G-protein-coupled receptors. Nature *429*, 188-193.Holmström, K.M., and Finkel, T. (2014).

Cellular mechanisms and physiological consequences of redox-dependent signalling. Nature Reviews Molecular Cell Biology *15*, 411-421.

Hsieh, J.-Y., Wang, H.-W., Chang, S.-J., Liao, K.-H., Lee, I.-H., Lin, W.-S., Wu, C.-H., Lin, W.-Y., and Cheng, S.-M. (2013). Mesenchymal stem cells from human umbilical cord express preferentially secreted factors related to neuroprotection, neurogenesis, and angiogenesis. PloS One *8*, e72604.

Hu, J., Li, T., Du, S., Chen, Y., Wang, S., Xiong, F., and Wu, Q. (2015). The MAPK signaling pathway mediates the GPR91-dependent release of VEGF from RGC-5 cells. International Journal of Molecular Medicine *36*, 130-138.

Husted, A.S., Trauelsen, M., Rudenko, O., Hjorth, S.A., and Schwartz, T.W. (2017). GPCR-Mediated Signaling of Metabolites. Cell Metabolism *25*, 777-796.

Ishikawa, K., Takenaga, K., Akimoto, M., Koshikawa, N., Yamaguchi, A., Imanishi, H., Nakada, K., Honma, Y., and Hayashi, J.-I. (2008). ROS-generating mitochondrial DNA mutations can regulate tumor cell metastasis. Science *320*, 661-664.

Jheng, H.-F., Tsai, P.-J., Guo, S.-M., Kuo, L.-H., Chang, C.-S., Su, I.-J., Chang, C.-R., and Tsai, Y.-S. (2012). Mitochondrial fission contributes to mitochondrial dysfunction and insulin resistance in skeletal muscle. Molecular and Cellular Biology *32*, 309-319.

Kaksonen, M., Toret, C.P., and Drubin, D.G. (2006). Harnessing actin dynamics for clathrin-mediated endocytosis. Nature reviews Molecular Cell Biology *7*, 404-414.

Kim, D.I., Lee, K.H., Gabr, A.A., Choi, G.E., Kim, J.S., Ko, S.H., and Han, H.J. (2016). Aβ-Induced Drp1 phosphorylation through Akt activation promotes excessive mitochondrial fission leading to neuronal apoptosis. Biochimica et Biophysica Acta -Molecular Cell Research *1863*, 2820-2834.

Kim, H.J., Shaker, M.R., Cho, B., Cho, H.M., Kim, H., Kim, J.Y., and Sun, W. (2014). Dynamin-related protein 1 controls the migration and neuronal differentiation of subventricular zone-derived neural progenitor cells. Scientific Reports *5*, 15962-15962.

Lee, H.J., Ryu, J.M., Jung, Y.H., Oh, S.Y., Lee, S.J., and Han, H.J. (2015). Novel Pathway for Hypoxia-Induced Proliferation and Migration in Human Mesenchymal Stem Cells: Involvement of HIF-1alpha, FASN, and mTORC1. Stem Cells *33*, 2182-2195.

Li, Y.H., Woo, S.H., Choi, D.H., and Cho, E.-H. (2015). Succinate causes α-SMA production through GPR91 activation in hepatic stellate cells. Biochemical and Biophysical Research Communications *463*, 853-858.

Maxson, S., Lopez, E.A., Yoo, D., Danilkovitch-Miagkova, A., and LeRoux, M.A. (2012). Concise review: role of mesenchymal stem cells in wound repair. Stem Cells Translational Medicine *1*, 142-149.

Mills, E., and O' Neill, L.A.J. Succinate: a metabolic signal in inflammation. Trends in Cell Biology *24*, 313-320.

Mu, X., Zhao, T., Xu, C., Shi, W., Geng, B., Shen, J., Zhang, C., Pan, J., Yang, J., and Hu, S. (2017). Oncometabolite succinate promotes angiogenesis by upregulating VEGF expression through GPR91-mediated STAT3 and ERK activation. Oncotarget *5*.

Murphy, M.B., Moncivais, K., and Caplan, A.I. (2013). Mesenchymal stem cells: environmentally responsive therapeutics for regenerative medicine. Experimental & Molecular Medicine *45*, e54.

Nasrallah, C.M., and Horvath, T.L. (2014). Mitochondrial dynamics in the central regulation of metabolism. Nature Reviews Endocrinology *10*, 650-658.

Panieri, E., and Santoro, M.M. (2015). ROS signaling and redox biology in endothelial cells. Cellular and Molecular Life Sciences *72*, 3281-3303.

Pell, V.R., Chouchani, E.T., Frezza, C., Murphy, M.P., and Krieg, T. (2016). Succinate metabolism: a new therapeutic target for myocardial reperfusion injury. Cardiovascular Research, cvw100.

Prieto, J., Leon, M., Ponsoda, X., Sendra, R., Bort, R., Ferrer-Lorente, R., and Raya, A. (2016). Early ERK1/2 activation promotes DRP1-dependent mitochondrial fission necessary for cell reprogramming. Nature *7*, 11124.

Rubic, T., Lametschwandtner, G., Jost, S., Hinteregger, S., Kund, J., Carballido-Perrig, N., Schwärzler, C., Junt, T., Voshol, H., and Meingassner, J.G. (2008). Triggering the succinate receptor GPR91 on dendritic cells enhances immunity. Nature Immunology *9*, 1261-1269.

Ryu, C.H., Park, S.A., Kim, S.M., Lim, J.Y., Jeong, C.H., Jun, J.A., Oh, J.H., Park, S.H., Oh, W.-i., and Jeun, S.-S. (2010). Migration of human umbilical cord blood mesenchymal stem cells mediated by stromal cell-derived factor-1/CXCR4 axis via Akt, ERK, and p38 signal transduction pathways. Biochemical and Biophysical Research Communications *398*, 105-110.

Schrepfer, E., and Scorrano, L. (2016). Mitofusins, from Mitochondria to Metabolism. Molecular Cell *61*, 683-694.

Suh, H.N., and Han, H.J. (2015). Sonic hedgehog increases the skin wound-healing ability of mouse embryonic stem cells through the microRNA 200 family. British Journal of Pharmacology *172*, 815-828.

Sundström, L., Greasley, P.J., Engberg, S., Wallander, M., and Ryberg, E. (2013). Succinate receptor GPR91, a Gαi coupled receptor that increases intracellular calcium concentrations through PLCβ. FEBS Letters *587*, 2399-2404.

Taguchi, N., Ishihara, N., Jofuku, A., Oka, T., and Mihara, K. (2007). Mitotic phosphorylation of dynamin-related GTPase Drp1 participates in mitochondrial fission. Journal of Biological Chemistry *282*, 11521-11529.

TeSlaa, T., Chaikovsky, A.C., Lipchina, I., Escobar, S.L., Hochedlinger, K., and Huang, J. (2016). a-Ketoglutarate Accelerates the Initial Differentiation of Primed Human Pluripotent Stem Cells. Cell Metabolism *24*, 1-9.

Todeschi, M.R., El Backly, R., Capelli, C., Daga, A., Patrone, E., Introna, M., Cancedda, R., and Mastrogiacomo, M. (2015). Transplanted umbilical cord mesenchymal stem cells modify the in vivo microenvironment enhancing angiogenesis and leading to bone regeneration. Stem Cells and Development *24*, 1570-1581.

Trudeau, K., Molina, A.J., and Roy, S. (2011). High glucose induces mitochondrial morphology and metabolic changes in retinal pericytes. Investigative Ophthalmology & Visual Science *52*, 8657-8664.

Wanet, A., Arnould, T., Najimi, M., and Renard, P. (2015). Connecting Mitochondria, Metabolism, and Stem Cell Fate. Stem Cells and Development *24*, 1957-1971.

Wang, W., Wang, Y., Long, J., Wang, J., Haudek, S.B., Overbeek, P., Chang, B.H., Schumacker, P.T., and Danesh, F.R. (2012). Mitochondrial fission triggered by hyperglycemia is mediated by ROCK1 activation in podocytes and endothelial cells. Cell Metabolism *15*, 186-200.

Wang, X., Ge, J., Tredget, E.E., and Wu, Y. (2013). The mouse excisional wound splinting model, including applications for stem cell transplantation. Nature Protocols *8*, 302-309.

Wang, Y., Zang, Q.S., Liu, Z., Wu, Q., Maass, D., Dulan, G., Shaul, P.W., Melito, L., Frantz, D.E., and Kilgore, J.A. (2011). Regulation of VEGF-induced endothelial cell migration by mitochondrial reactive oxygen species. American Journal of Physiology-Cell Physiology *301*, C695-C704.

Yu, T., Robotham, J.L., and Yoon, Y. (2006). Increased production of reactive oxygen species in hyperglycemic conditions requires dynamic change of mitochondrial morphology. Proceedings of the National Academy of Sciences of the United States of America *103*, 2653-2658.

Yu, Y., Dumollard, R., Rossbach, A., Lai, F.A., and Swann, K. (2010). Redistribution of mitochondria leads to bursts of ATP production during spontaneous mouse oocyte maturation. Journal of Cellular Physiology *224*, 672-680.

국 문 초 록

숙신산에 의한 DRP1 인산화에 의해 유도되는 미토콘드리아 분절이 인간 중간엽 줄기세포 이동에 미치는 영향

서울대학교 대학원

수의학과 수의생명과학 전공

고 소 희

지도교수 한 호 재

줄기세포 대사물질들은 세포 증식이나 이동과 같은 줄기세포 행동을 조절하고 있는 것으로 알려져 있다. 최근 들어 줄기세포 대사물질들이 신호전달 물질로서 작용한다는 것이 보고되고 있다. 또한, 세포 대사 조

절 과정에서 미토콘드리아 형태가 중요한 역할을 하고 있음이 알려져 있다. 그러나 줄기세포 대사산물이 미토콘드리아 형태 변화를 통해 어떻게 줄기세포 이동을 조절하는지는 명확하게 밝혀지지 않았다. 본 연구의 목적은 줄기세포 대사산물인 숙신산이 미토콘드리아 역학 관련 단백질에 대한 조절을 통해 인간 유래 중간엽 줄기세포 이동에 어떻게 관여하는지에 대해 규명하는 것이다. 본 연구에서는 인간 유래 제대혈 줄기세포, western blotting, co-immunoprecipitation, siRNA transfection, confocal microscopy, fluocytometer를 이용하였다. 그 결과는 다음과 같다.

숙신산은 줄기세포 이동을 GPR91를 통하여 유의적으로 증가시켰다. 또한 숙신산은 $G\alpha_q$ 과 $G\alpha_{12}$ 를 통하여 PKCζ 인산화를 증가 시켰다. 활성화된 PKCζ는 p38 MAPK을 인산화 시켰으며, 이는 미토콘드리아 역학 단백질인 DRP1을 인산화 시켜 미토콘드리아 분절을 유발하였다. 숙신산에 의한 미토콘드리아 분절은 미토콘드리아 기능에 영향을 미쳐, 세포 내 ATP 양, 미토콘드리아 막전위, 미토콘드리아에서 생성되는 ROS의 증가를 유도하는 것으로 관찰되었다. 증가된 미토콘드리아 ROS는 Rho GTPase들을 활성화 시키고, F-actin 형성을 증가시켰다. 피부 상처 치유 모델에서, 숙신산을 전 처리한 줄기세포 처리 군이 대조군과 비교하여 혈관 재형성 및 재 상피화의 속도를 증가시켜 더 빠른 상처 치유를 유도하였고, 이는 *drp1* siRNA 처리군에서 모두 감소되었다.

결론적으로 숙신산은 GPR91 수용체를 통해 PKCζ/p38 MAPK을 활성화시켰으며, 활성화된 p38은 DRP1을 인산화하여 미토콘드리아 분절을 일으켰다. 미토콘드리아 분절에 의한 미토콘드리아 ATP 생산 및 막전위의 증가는 미토콘드리아 ROS 발생을 유도하였으며 Rho GTPase를 활성화하고 결국 F-actin 형성 촉진을 통하여 줄기세포 이동을 향상시켜 상처치유속도를 증가시켰다.

주요어 : 숙신산, GPR91, 미토콘드리아 역학, DRP1, p38 MAPK, 활성산소, 인간 유래 중간엽 줄기세포

학번 : 2015-21807